2009-01-01

Microstructural Characterization and Heat Treatment of A-286 Turbine Buckets

Christopher Michael Bradley
University of Texas at El Paso, cbradley2@miners.utep.edu

MICROSTRUCTURAL CHARACTERIZATION AND HEAT TREATMENT OF A-286 TURBINE BUCKETS

CHRISTOPHER MICHAEL BRADLEY

Department of Metallurgical and Materials Engineering

APPROVED:

_____
Luis Trueba, Ph.D., Chair

_____
Stephen W. Stafford, Ph.D.

_____
Wen Whai Li, Ph.D.

_____
Patricia D. Witherspoon, Ph.D.
Dean of the Graduate School

MICROSTRUCTURAL CHARACTERIZATION AND HEAT TREATMENT OF A-286 TURBINE BUCKETS

By

CHRISTOPHER MICHAEL BRADLEY

THESIS

Presented to the Faculty of the Graduate School of

The University of Texas at El Paso

in Partial Fulfillment

of the Requirements

for the Degree of

MASTER OF SCIENCE

Department of Metallurgical and Materials Engineering

THE UNIVERSITY OF TEXAS AT EL PASO

August 2009

Abstract

A-286 is an iron-based superalloy used extensively in land-based gas turbines for 2nd stage (low pressure) buckets and 1st and 2nd stage wheels. Although A-286 may appear to some as just another austenitic stainless steel, its elevated temperature properties are attributed to γ' precipitate structures, effective distributions of alloy carbides in the forms of $M_{23}C_6$, M_6C and MC, and solid solution strengthening. Unfortunately over the course of these components service lives microstructural degradation develops in the form of η-phase formation. The presence of η-phase, especially in large quantities, can have a negative effect on stress rupture properties. Resistance to creep rupture and dimensional stability are desirable elevated temperature properties necessary for turbine operational capacity. Since a significant portion of the elevated temperature strength of A-286 is accomplished by the formation of ordered FCC γ' precipitates, utilizing alloy additions of aluminum and titanium, the deleterious η-phase formation depletes the alloy of γ' particles. This investigation presents the use of in-situ metallography, optical microscopy and scanning electron microscopy to quantify the severity of η-phase formation in its microstructural forms and distribution. Recognizing that gas turbine operators extend the service lives of these components beyond warranty coverage, this research should aid in engineering decisions involving the re-use of these A-286 components. This research also has explored the potential for rehabilitation of A-286 turbine buckets, which have demonstrated the formation of η-phase. Through a solutionizing and aging heat treatment, η-phase can be restored back into a "near new" microstructural state, extending the service life of these various components.

Table of Contents

List of Tables

List of Figures

Introduction

The superalloy A-286 is an iron-based alloy commonly used for turbine applications that consists of an austenitic (γ) face centered cubic (FCC) structure. Although A-286 may appear to some as just another austenitic stainless steel, its elevated temperature properties are attributed to γ' precipitate structures, effective distributions of alloy carbides in the forms of $M_{23}C_6$, M_6C and MC, and solid solution strengthening. Turbine wheels and buckets should have ASTM grain sizes ranging from 4 to 6 which designate medium grain sizes that are desirable for polycrystalline turbine components. ASTM grain sizes ranging from 8-10 would designate finer grains which are undesirable for elevated temperature conditions due to large grain boundary surface areas allowing for more grain boundary sliding.

Turbine buckets, or airfoils, need to be able to withstand longitudinal (axial) stresses approximately 20,000 psi and temperatures in the range of 650-980°C. The bucket root which attaches to the turbine wheel can experience stresses around 40,000-80,000 psi and a temperatures near 760°C or lower because this section is outside of the hot gas path.[1] Bucket root stress conditions would coincide with flexural or torsional movements of the bucket in service. According to AMS 5737, minimum tensile strengths at room temperature that would have to be satisfied are 140,000 psi with yield strength of 95,000 psi. Hardness measurements should be in the 277-363 Brinell hardness (Vickers 292-392) range, but the product shall not be rejected on the basis of hardness if the tensile property requirements are met.[2] To maintain efficiency of the turbine, dimensional stability and excellent resistance to creep rupture are also

important. The alloy additions allow this alloy to achieve the high temperature properties of this material through solid solution strengthening, precipitation hardening, dispersion hardening (carbides) and grain boundary strengthening. Figure 1.1 and 1.2 shows a GE Frame 3 land-based gas turbine in which A-286 buckets are extensively used for 2nd stage (low pressure) buckets and 1st and 2nd stage wheels.

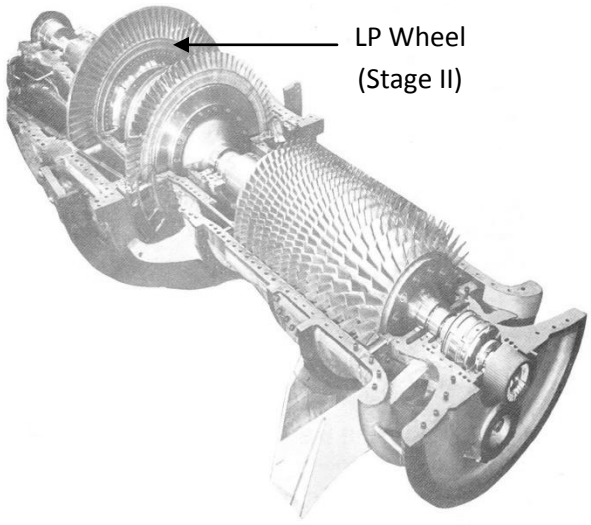

Figure 1.1: GE Frame 3 gas turbine

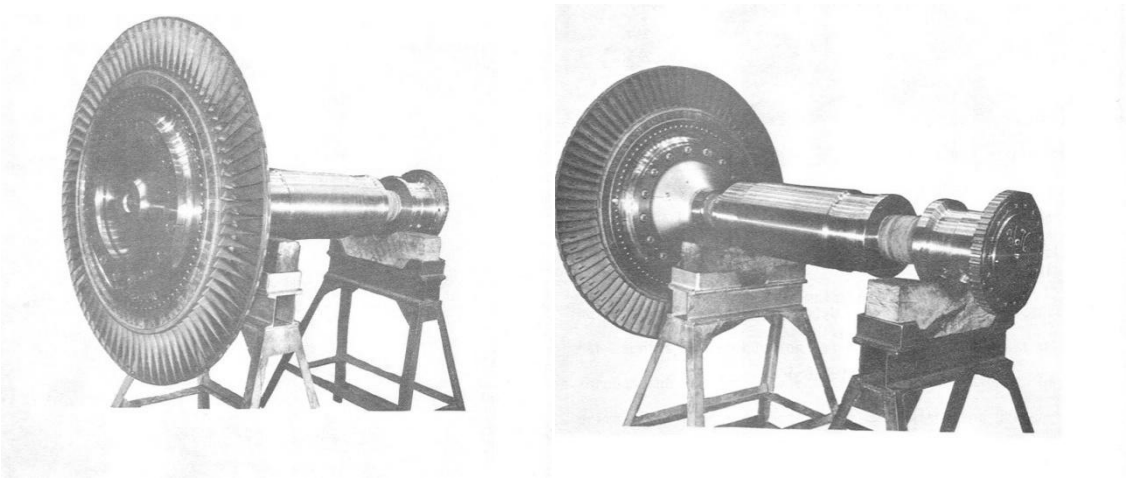

Figure 1.2: Front view (left) and Rear view (right) of the low pressure (load) turbine wheel.

The increased amount of nickel in the austenitic iron matrix improves stability and permits more alloying without the formation of deleterious phases.[3] The strengthening of A-286 is accomplished by ordered FCC γ', which precipitates from the γ matrix below 860°C, in what is considered an iron-rich alloy. Precipitation strengthening is dependent on the additions of titanium and aluminum, which are normally less than 2 wt%. The γ' phase forms coherently on the {100} matrix planes.[4] The minimum nickel addition needed to maintain an austenite matrix is roughly 25 wt % due to low carbon content (< 0.1 wt %) and large amounts of ferrite stabilizers (chromium and molybdenum). The additions of chromium and molybdenum partition preferentially to γ, playing a number of roles that have important effects. Molybdenum and chromium are carbide formers, and they reduce the matrix solubility for the precipitation-strengthening elements such as titanium and aluminum, resulting in little or no precipitation in the absence of molybdenum and chromium.[2]

Additions of the solid solution strengtheners, chromium and molybdenum result in a lattice distortion which can impose a coherency strain between the matrix and the precipitates. In order to minimize the lattice distortion between the matrix and the precipitate it is necessary to have a high Ti/Al ratio. This is important because if the Ti/Al ratio becomes greater than 2:1 then γ' will transform to a hexagonal closed-packed (HCP) η-phase which can form with long-term elevated service conditions. Solid solution strengtheners also play a role in reducing stacking fault energies which impede cross-slip at elevated temperatures thus leading to improved creep resistance.

Chromium plays a role in the corrosion-oxidation resistance allowing use of turbines in aggressive elevated-temperature environments. Boron and vanadium are both added to improve hot workability. Also, boron enhances creep rupture properties at the grain boundaries by forming borides that help prevent grain boundary sliding. Boron has been shown to inhibit the transition of γ' to the unfavorable η-phase by delaying nucleation at the grain boundaries.[5] Table 1.1 shows the minimum and maximum chemical compositions of A-286.

Table 1.1: Composition of A-286.[6]

Element	Min %	Max %	Purpose
Chromium (Cr)	13.50	16.00	BCC stabilizer, corrosion/oxidation resistance, carbide former
Nickel (Ni)	24.00	27.00	FCC stabilizer, γ' former
Molybdenum (Mo)	1.00	1.50	Carbide former
Vanadium (V)	0.10	0.50	Strengthener and improves hot workability
Aluminum (Al)	-	0.35	γ' former, inhibits η formation
Titanium (Ti)	1.90	2.35	Strengthener, carbide former
Boron (B)	0.003	0.010	Improves grain boundary morphology
Carbon (C)	-	0.08	Promotes strength in grain boundaries, FCC stabilizer
Iron (Fe)	Balance		FCC matrix

Intergranular carbides prevent grain boundary sliding, which increase creep strength and help maintain dimensional stability. If no carbides are present, excessive grain-boundary sliding leads to premature failure. Being titanium rich, A-286, contains MC (TiC) carbides which are normally irregular in shape, and precipitate along the γ–grain boundaries during processing, heat treatment or service. These carbides promote good rupture life, but can form films that can cause embrittlement and should be avoided during processing or service. M_6C carbides form in the γ-grain boundaries and require enough molybdenum to form Mo_6C which normally occurs during solidification or heat treatment. Another important carbide in this alloy's structure is $M_{23}C_6$, which is predominantly chromium ($Cr_{23}C_6$) and is also formed in the γ-grain boundaries. Formation can occur during processing, heat treatment or service and can have a negative effect on stress rupture sensitivity if it is improperly processed due to a cellular film formation.

The strength of the alloy is related to the gamma prime phase (γ') by the volume fraction of γ', particle size of γ', coherency strains between γ-γ', the antiphase boundary (APB) and stacking fault energies (SFE) of γ'. Finer, more evenly dispersed γ' results in more effective strengthening. At a constant volume fraction (V_f) of γ', the strength of the material increases as the particle size increases, until a certain particle size is reached. The volume fraction of γ' in A-286 ranges from 0.095 after two hours to 0.107 after 100 hours at 720°C. This volume fraction forms early in aging and the aging strength increase is strongly correlated with increasing precipitate particle size up to a maximum aging hardness. After peak hardening, further particle growth causes decreased strength since dislocations will then bypass the particles by looping around them due to the lack of coherency at the particle/matrix interface. Particle coarsening is most likely controlled by the diffusion of titanium through the matrix.[2]

Typical heat treatments for A-286 include a solution anneal at either 900°C for 2 hours or 980°C for 1 hour, oil quench, followed by aging at 715°C for 16 hours and an air cool. The 900°C solution treatment results in a finer grain size and superior short time tensile properties at room and elevated temperatures compared to the 980°C solution treatment. A two-cycle aging treatment is occasionally specified after the 900°C solution treatment. This treatment consists of aging at 700-760°C for 16 hours, air cooling to room temperature, another aging treatment at 650°C for 8-12 hours and finally air cooling to room temperature. This procedure is intended to improve notch rupture strength. The 980°C solution treatment develops a slightly coarser grain size with superior creep-rupture properties. In the aging process, precipitates form in a dispersed arrangement throughout the matrix. Finer grain sizes will improve tensile and

fatigue properties, while a coarse grain structure will improve creep rupture properties at the cost of lower tensile strength and fracture toughness. Creep rupture properties improve because of a decrease in grain boundary surface area, which reduces the amount of grain boundary sliding. These properties can be controlled through processing during forging and subsequent heat treatments. Overaging the alloy tends to cause ripening or coarsening of the precipitates creating a transformation of γ' to η. This causes a loss in alloy properties such as tensile strength and stress rupture life resulting from the dislocations looping around and between the particles.[7]

During elevated temperature conditions, A-286 tends to form a phase deleterious to the alloy by depleting γ' from the matrix. This phase is known as Ni_3Ti (η). Eta-phase (η) can form in the processing and manufacturing of A-286 in the heat treatment stages (forging and aging) and can also form during long-term elevated service conditions. There are two forms that may occur, intergranular platelets that form by way of γ'-η transformation (sometimes with a Widmanstätten form) and a cellular grain boundary (pearlitic) form. Extended exposures of A-286 to temperatures in the 1100°C-1560°C range results in the formation of cellular η-phase. This precipitate appears as an alternate coherent lamellar of η and γ originating at the γ-grain boundary with a random orientation to the grain in which the cellular zone is growing. Exposure to temperatures greater than 800°C causes coarse intergranular platelet formations of η-phase. This formation can best be avoided if heat treatments are above the η-solvus of 915°C and if the alloy is utilized below the gamma prime→eta transformation temperature near 800°C. The coarse interlamellar spacing of η, as well as the loss of the more finely

distributed γ' in the matrix involved with cellular formation, often leads to severe degradation of mechanical properties, specifically the loss of stress rupture strength.

In an earlier investigation by Heydt, a cellular formation that created notch-sensitivity was performed to see if the formation was either $M_{23}C_6$ or η-phase. In the investigation it was observed that the austenite between the well developed lamellar structure of η-phase depletes the austenitic matrix of γ' leaving the matrix weak and ductile. Following studies of a poorly defined lamellar structure concluded that the austenite between the lamellae is more hard and brittle than the austenite found between the lamellae of η-phase. This poorly defined lamellar structure was concluded to be $M_{23}C_6$. With stress-rupture failures occurring intergranularly it is possible that the $M_{23}C_6$ is the cause for notch-sensitivity by making the austenite hard and brittle creating an easy path for a crack to propagate.[8,9]

During the aging process very little η-phase precipitation will occur because the intensity in which η-phase develops increases with titanium content. According to Clark and Pickering[10], cellular precipitation doesn't occur until the alloy is very near the maximum aged condition. The alloy started to overage when about 10-20% cellular precipitation was present in the structure. As the amount of cellular precipitation increased, the hardness decreased rapidly until the structure reached 100% cellular formation in which the hardness remained constant. The higher the aging temperature, the greater is the interlamellar spacing of η-phase in the cellular structure resulting in lower hardness. Increasing aging temperature or increasing titanium considerably accelerates the cellular formation process. Speich[11] showed that the interlamellar

spacing is inversely proportional to the degree of undercooling below the solubility limit of η in austenite.

The orientation relationship between η and γ is:

{0001}η//{111}γ

<1210>η//<110>γ

This is the orientation in correspondence to close-packed planes and close-packed directions in the lattices of each phase. Cellular precipitation occurs at the grain boundaries, and such a nucleus can only have an orientation relationship with one of the grains. The η-phase nucleation will have a low-energy interface with the grain in which it has the favored orientation relationship. With stability in the interface, η-phase will not be mobile and the accompanying recrystallization of austenite will occur into the grain where there is no well developed orientation relationship. The interface in the front of that cellular interface will be non-coherent possessing a high energy and will be very mobile leading to the side by side nucleation of the lamellar structure due to diffusion conditions.[12] The Widmanstätten structure starts with the transformation of γ' to η and this phenomenon occurs due to a relief of stress in rows of particles in <110> austenite directions. The rows will coalesce to define {111} austenite planes on which the η-phase plate grows. The orientation relationship of Widmanstätten and cellular forms of η-phase are the same.[10,12]

The exact temperature at which η-formation occurs is a strong function of the titanium level and alloy base chemistry. Increases in Ti and hot and cold work strain

energies enhance the η-formation in both cellular and Widmanstätten structures. The chemical state of A-286 can allow for slight modifications which may alleviate turbine components of η-phase formation. Aluminum is beneficial with inhibiting both forms of η-phase due to its' differential solubility in the η and γ' phases. Thus for increased aluminum additions it is less likely that adequate aluminum can be removed from a site such that η can nucleate and grow. Also, aluminum may decrease the $\gamma - \gamma$' mismatch, thus reducing the driving force for both intergranular and cellular η-phase formations. Trace levels of boron are commonly used to prevent η-phase formation. Equilibrium segregation of boron to the grain boundaries retards the nucleation of η-phase cells by occupying sites where η-phase can nucleate and grow and also increases notch stress rupture properties.

Cellular formations of η-phase can be regarded as a fairly stable form of dispersion hardening and has an incredible resistance to over-aging. This effect can be useful in maintaining high strength levels either during elevated service conditions or after high temperature aging. Unfortunately, with large amounts of cellular precipitation the ductility (creep ductility) is low.[13]

Turbine buckets are expensive, and the failure of a single turbine bucket could cost an operator millions of dollars in damage, downtime and possible injuries to staff. In addition, a company is likely to replace the buckets after the manufacture's service warranty has expired at a significant cost to the operator. A rejuvenation heat treatment would allow the operator to obtain the greatest value from the buckets and return them to "near new" conditions. After the buckets have been in service for a specified amount of time they could be rejuvenated by means of re-solutionizing followed by aging. Re-

solutionizing the buckets would allow η-phase to revert back into solution eliminating the detrimental effects on stress rupture properties. Aging will then re-establish the alloy's strengthening mechanisms through precipitation of γ' giving the alloy the same properties it had when it was originally manufactured. This could potentially save companies substantial amounts of money. During the solution treatment the η-phase reverts back into solution and then into γ' after aging, because of their similar structures the transformation of η→γ' is reversible. This would benefit any company looking for ways to extend the life of their turbine components.

If the amount of η-phase cannot be controlled solely by solutionizing, then the only course of action is to minimize η-phase formation by controlling alloy chemistry and fabrication practice.[2,13] Suppressing η-phase formation can be achieved either by adjusting the limit to which age hardening does not cause enough strain for cellular precipitation to occur, by reducing thermal stresses by slower cooling rates after solution treatment. Another method would be the addition of small amounts of elements such as boron which neutralize the grain boundary nucleation sites.[13]

Procedure

This investigation was conducted on two buckets that were previously in-service. The buckets were from the Stage II portion of a GE Frame 3 gas turbine. The first bucket “A” was in service for 188,000 hours while the second bucket “B” was in service for 56,000 hours. In situ metallography and acetate film replication was performed on each bucket in order to determine if η-phase was present, and to compare the relative amount of η-phase found in each bucket. Bucket “A” showed a greater amount of η-phase than bucket “B” as shown in Figure 2.1. A correlation between service exposure and the amount of η-phase was observed in the replicas. In situ metallography was used because it is a non-destructive test method, and the buckets would have been preserved if no η-phase were found. Since both buckets showed signs of η-phase formation, experiments were performed in order to determine if the phase could be dissolved and re-dispersed into the matrix through a solutionizing and aging heat treatment. Samples that were replicated were etched with a 30 ml hydrochloric acid and 10 ml nitric acid solution known as aqua regia. From Figure 2.1, Bucket “A” also happens to have a smaller grain structure than bucket “B”. Smaller grains could be a driving force for nucleation and growth of η-phase due to larger grain boundary surface area, which hosts the sites in η-formation.

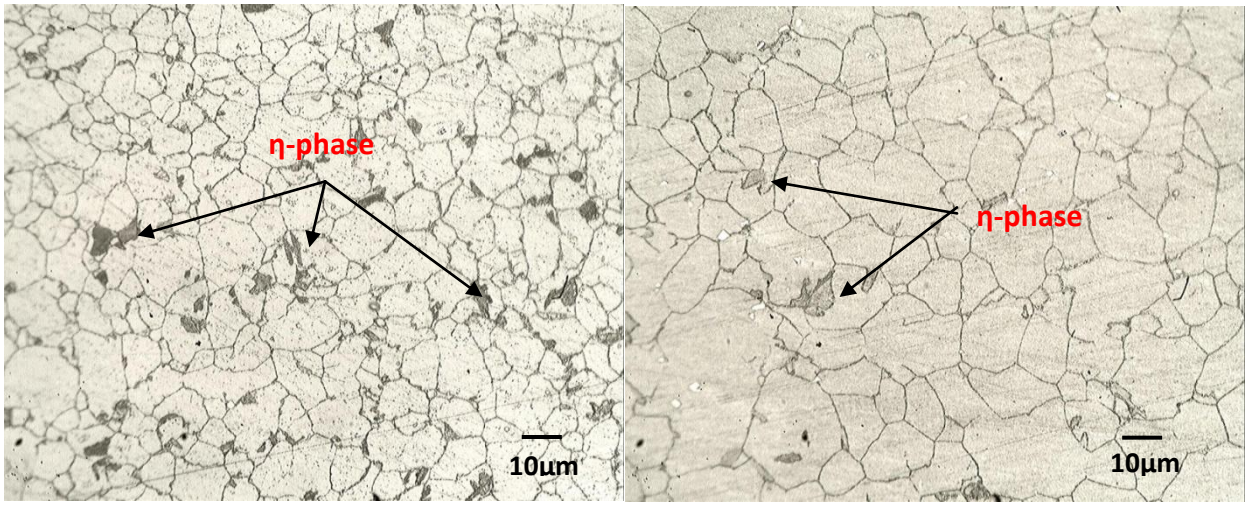

Figure 2.1: In-situ metallography and acetate film replication of airfoils. Arrows indicate the presence of η-phase on the surfaces of bucket "A" (left) and bucket "B" (right).

After confirming the presence of η-phase in the buckets, a heat treatment process was developed. The heat treatment process consisted of a solutionizing and aging heat treatment. The same solutionizing and aging times and temperatures used in manufacturing were used to evaluate whether or not the airfoils could be rejuvenated. Before heat treatment, the buckets were sectioned in order to distinguish if any microstructural changes occurred during the heat treatment process. The buckets were cut axially into thirds to determine the microstructure in the as-received, solutionized and aged conditions. The samples were then cut transversely into one-inch segments to determine how the microstructure changed along the temperature gradient acting on the airfoils during service conditions, as shown in Figure 2.2. There were a total of 48 samples (24 samples per bucket) that were prepared for optical microscopy by typical metallographic techniques. The buckets were sectioned using an

automated water jet cutter because of the poor machinability of A-286 and also to avoid frictional heating.

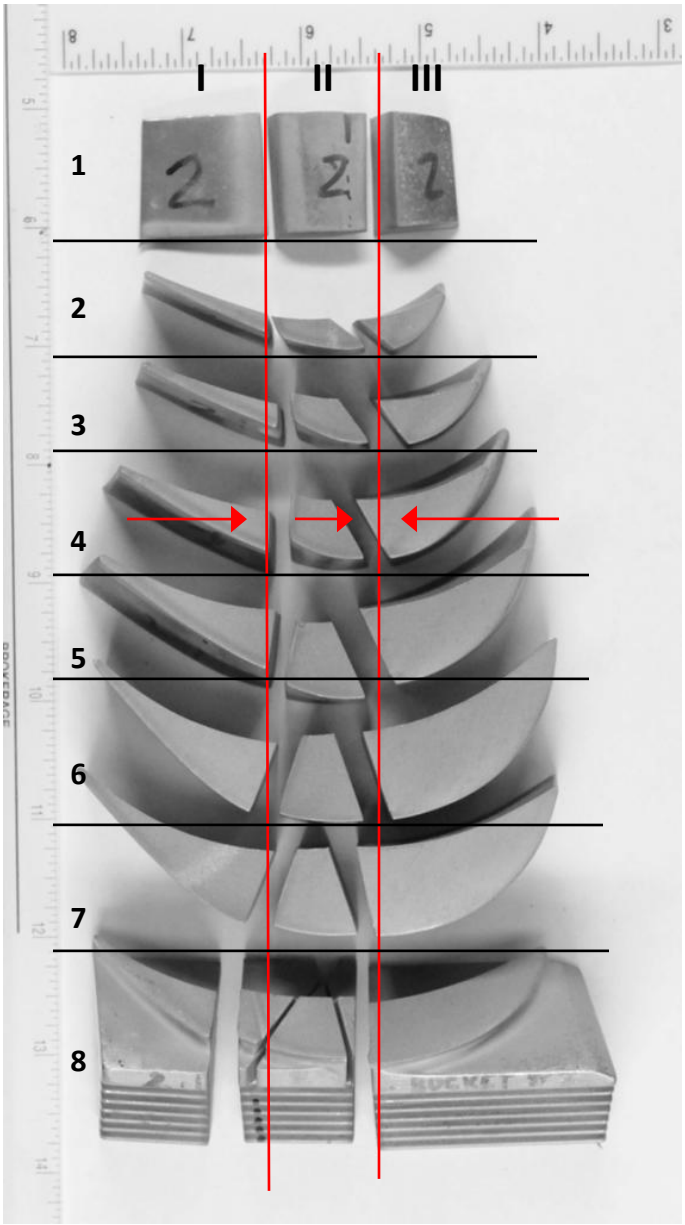

Figure 2.2: Sectioned bucket showing which specimens were examined in the as-received (I), solutionized (II), and solutionized and aged (III) conditions. The arrows designate the side of the bucket sections that were investigated via metallography.

Sections 1A (samples 1A1-1A8) and 1B (samples 1B1-1B8) were used as representative samples of the as-received condition. Metallography of these specimens revealed the microstructural state of the buckets after they were pulled from service. Scanning electron microscopy (SEM) was performed to further characterize phases such as carbides, γ' and η.

Sections 2A (samples 2A1-2A8) and 2B (2B1-2B8) were solutionized at 900°C for two hours in an argon atmosphere followed by an oil quench. The samples were inserted into a tube furnace at room temperature before the furnace was turned on it was purged with argon gas for two minutes. Once the furnace was purged the temperature controller was set to 900°C. The samples were in the furnace a total time of 140 minutes in which the first 30 minutes the furnace was ramping up to 900°C. Next the samples were pulled from the furnace and oil quenched. During the oil quench the samples were agitated to prevent nucleate boiling on the surface. Vapor at the surface of the samples would have decreased the rate of cooling. The samples were prepared for metallography to determine the effectiveness of solutionizing the η-phase into the matrix. Scanning electron microscopy was also performed on the re-solutionized samples to see if η-phase had gone into solution in the matrix.

Sections 3A (samples 3A1-3A8) and 3B (samples 3B1-3B8) were solutionized at 900°C for two hours and then cooled with an oil quench. In addition to this processing, they were aged at 720°C for 16 hours and then air cooled. The samples were inserted into a tube furnace at room temperature and the furnace was purged with argon gas for two minutes. Once the furnace was purged it was turned on and the temperature was set for 900°C. The samples were in the furnace a total time of 140 minutes in which the

first 30 minutes the furnace was ramping up to 900°C. Next the samples were removed from the furnace and oil quenched with agitation. The samples were then cleaned of any oil residue and prepared for the aging process. The samples were inserted into the furnace at room temperature and the furnace was purged with argon again for two minutes. The furnace was then set for 720°C; it took the furnace about 20-30 minutes to reach the designated temperature. The samples were left in the furnace for 16 hours and then removed from the furnace and allowed to air cool.

After cooling, the samples were prepared for optical microscopy using standard metallographic techniques. Both optical microscopy and SEM evaluations were used to determine if the re-solutionized and aged samples had a lower quantity of η-phase than the as-received samples and to determine what microstructural changes occurred during the aging process. The scanning electron microscopy and energy dispersive x-ray spectroscopy (EDS) were used to determine the phases present such as η-phase, γ' and various carbides (TiC, Mo_6C and $Cr_{23}C_6$).

Results

As-received microstructures of the Section I specimens are presented in Figures 3.1-3.16, the specimens start at the tip of the bucket in Figures 3.1 and 3.2 and transition down to the dovetail section in Figures 3.15 and 3.16. It was observed that there is a greater amount of η-phase at the tip compared to the dovetail region. This is due to the thermal gradient that the bucket experiences while in service; temperatures are expected to be higher at the bucket tip than the dovetail region of the airfoil. Also, as previously observed from the replicated samples, Airfoil "A" has a greater amount of η-phase than airfoil "B". This is expected because of the longer service life of airfoil "A".

Notice that in the previous optical microscopy pictures for replication that there is a noticeable difference in grain size between Airfoil A and Airfoil B. Airfoil A has a smaller grain size which could lend itself to a higher probability for η-phase formation due to the larger grain boundary surface area. Large grain boundary surface areas will result in greater number of sites which η-phase formation can nucleate and grow. The following equation was used to calculate the ASTM grain size for both buckets. Bucket "A" had an ASTM grain size of 7.26 and bucket "B" had an ASTM grain size of 6.4. Both buckets ASTM grain size values are slightly larger than the desirable ASTM grain size range of 4 to 6.

$$N\left(\frac{M}{100}\right) = 2^{n-1}$$

Using the line intercept method for calculating grain sizes, bucket “A” had an average grain size of 9 μm and bucket “B” had an average grain size of 11.8 μm.

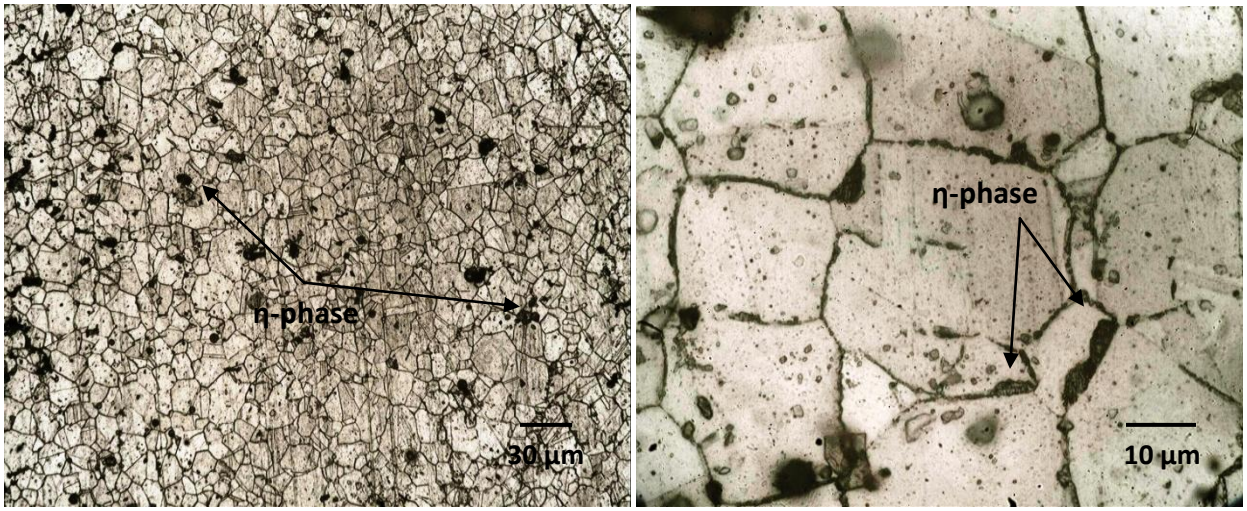

Figure 3.1: Sample 1A1. Arrows indicate the presence of η-phase (Kalling’s #2 etch).

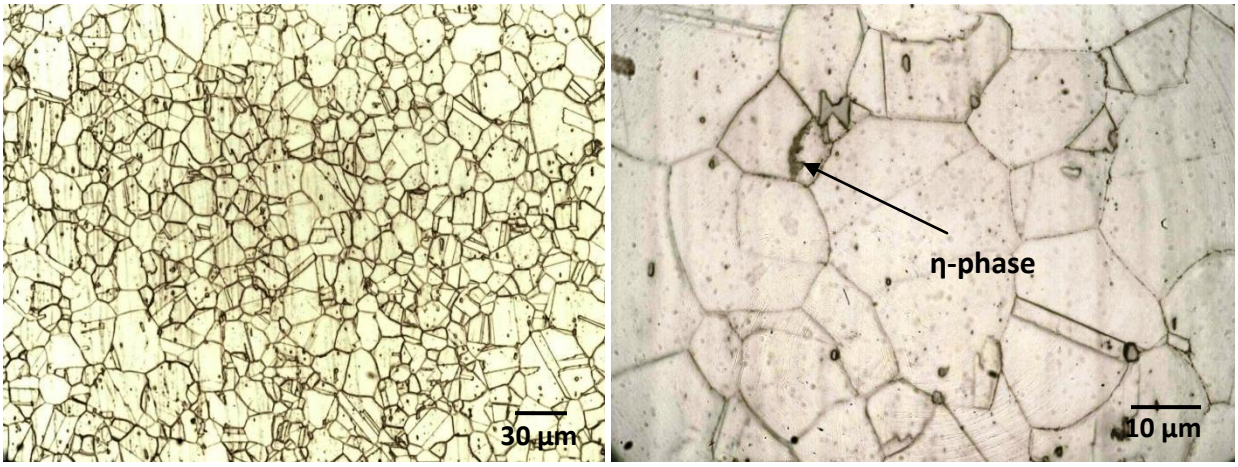

Figure 3.2: Sample 1B1. Arrow indicates the presence of η-phase (Kalling’s #2 etch).

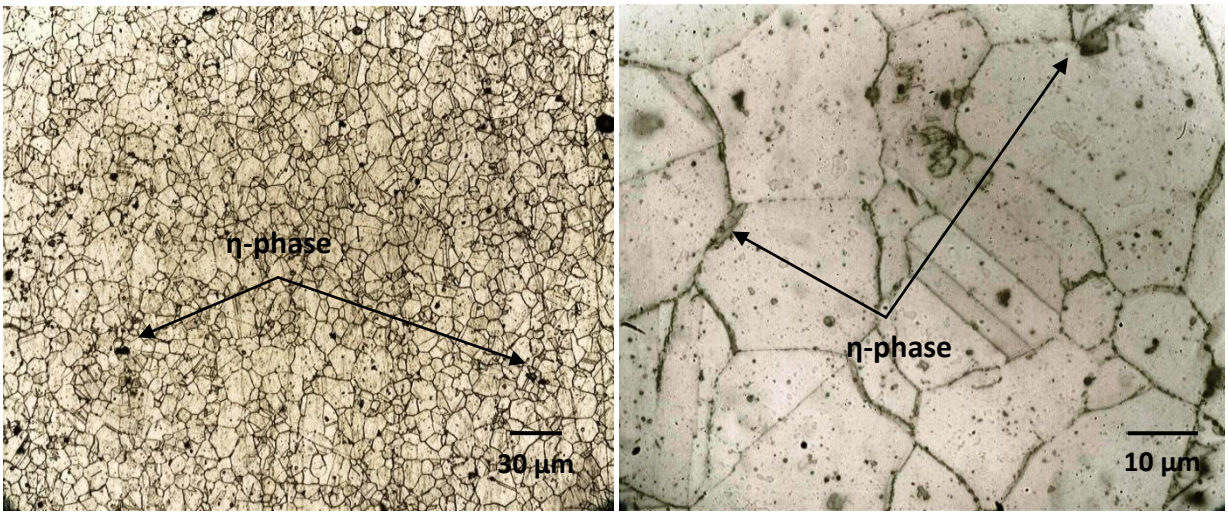

Figure 3.3: Sample 1A2. Arrows indicate the presence of η-phase (Kalling's #2 etch).

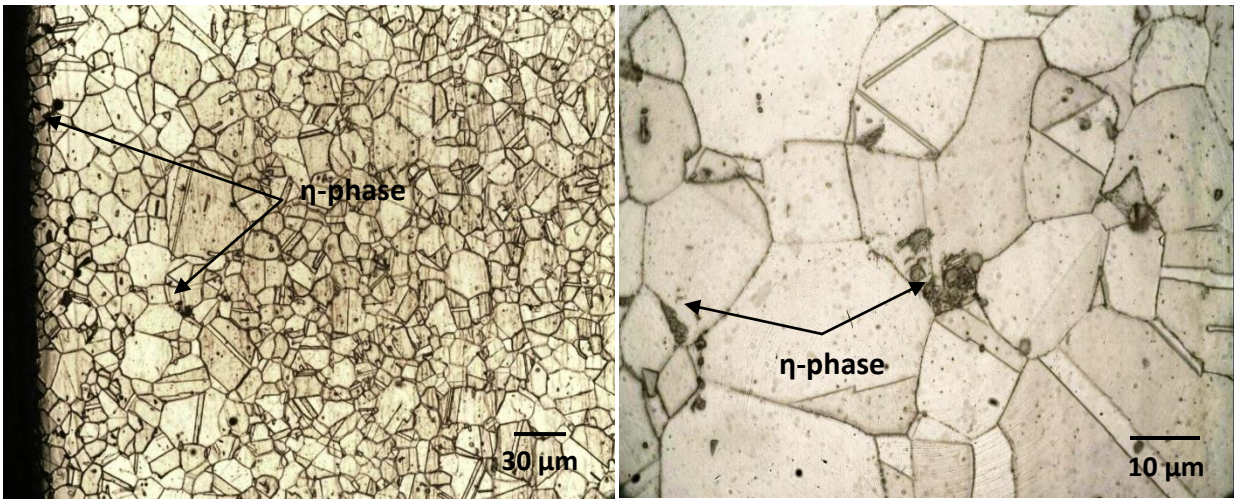

Figure 3.4: Sample 1B2. Arrows indicate the presence of η-phase near the surface of the airfoil (Kalling's #2 etch).

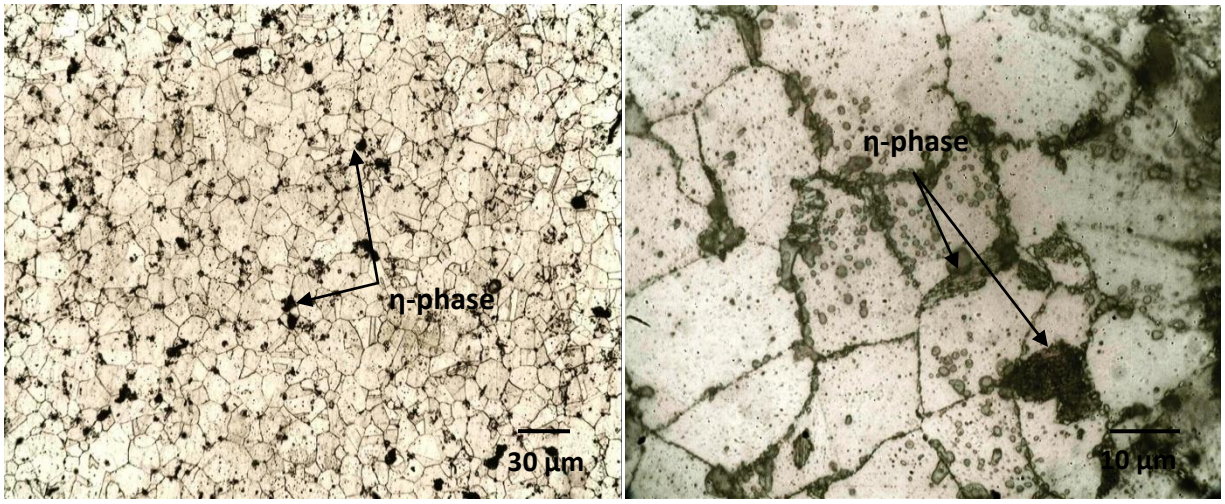

Figure 3.5: Sample 1A3. Arrows indicate the presence of η-phase (Kalling's #2 etch).

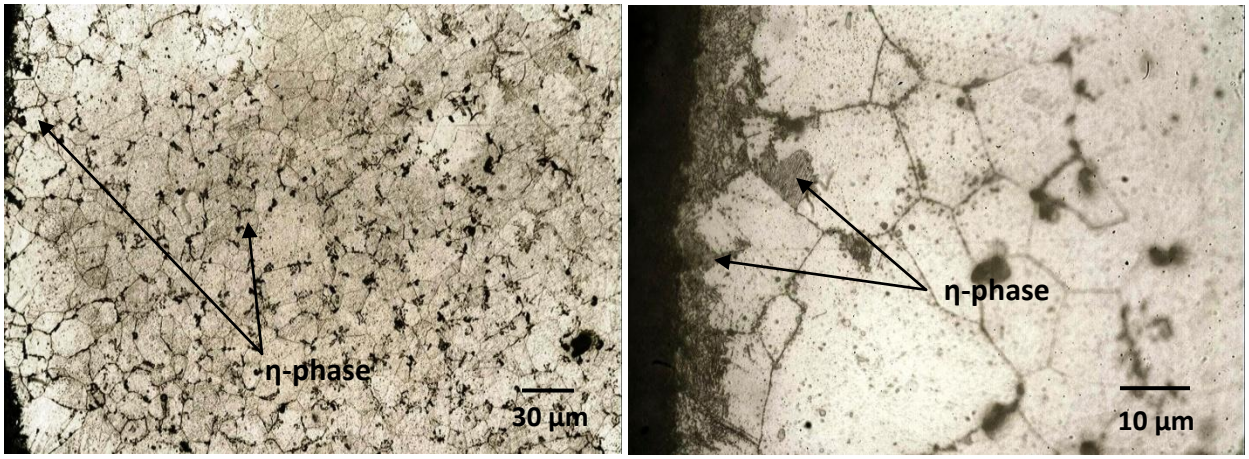

Figure 3.6: Sample 1B3. Arrows indicate the presence of η-phase on the airfoil surface (Kalling's #2 etch).

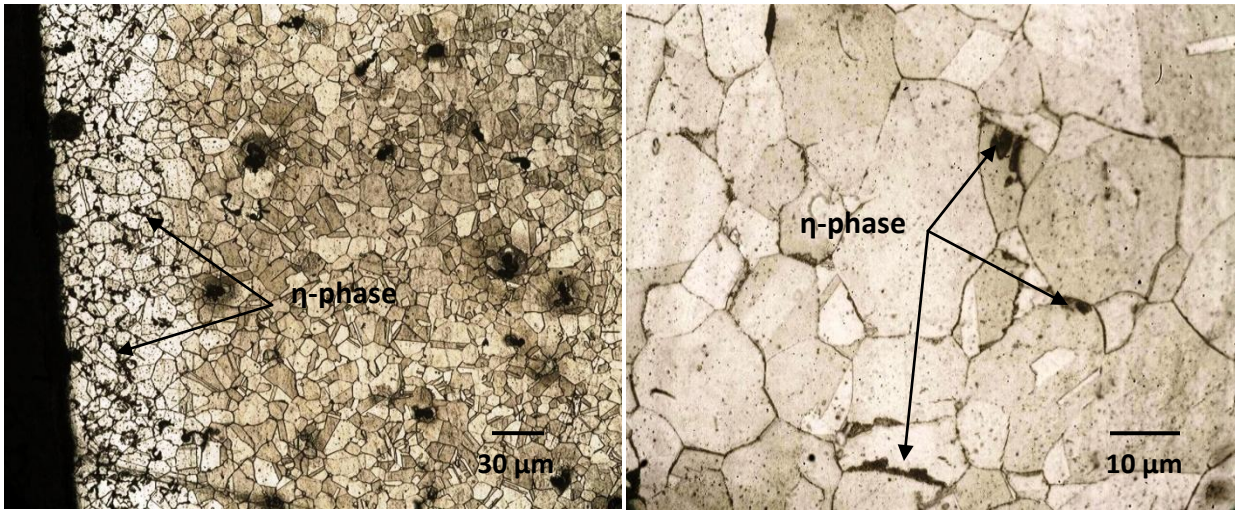

Figure 3.7: Sample 1A4. Arrows indicate the presence of η-phase near the surface region (Kalling's #2 etch).

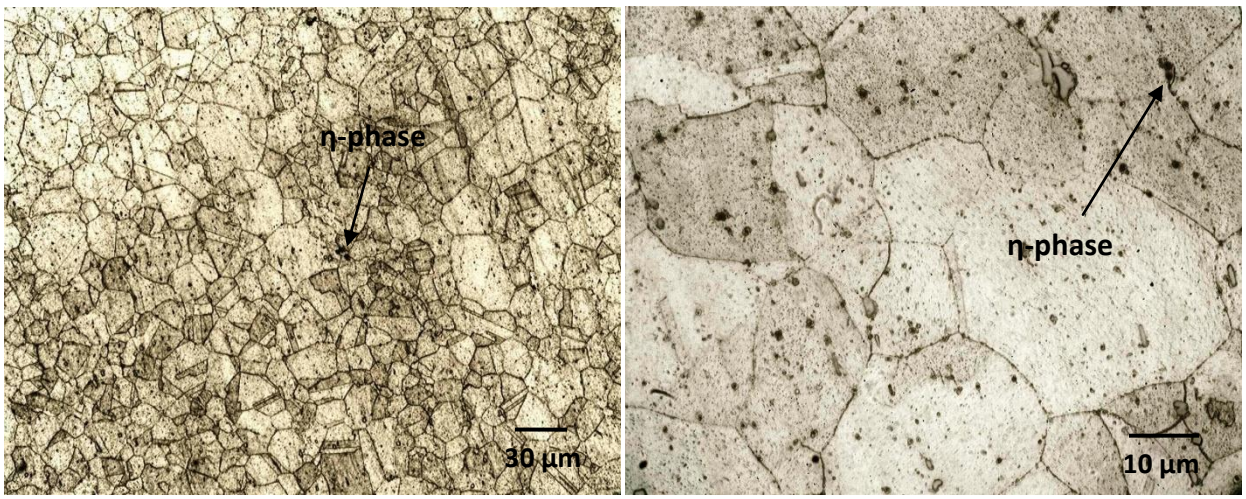

Figure 3.8: Sample 1B4. Arrows indicate the presence of η-phase (Kalling's #2 etch).

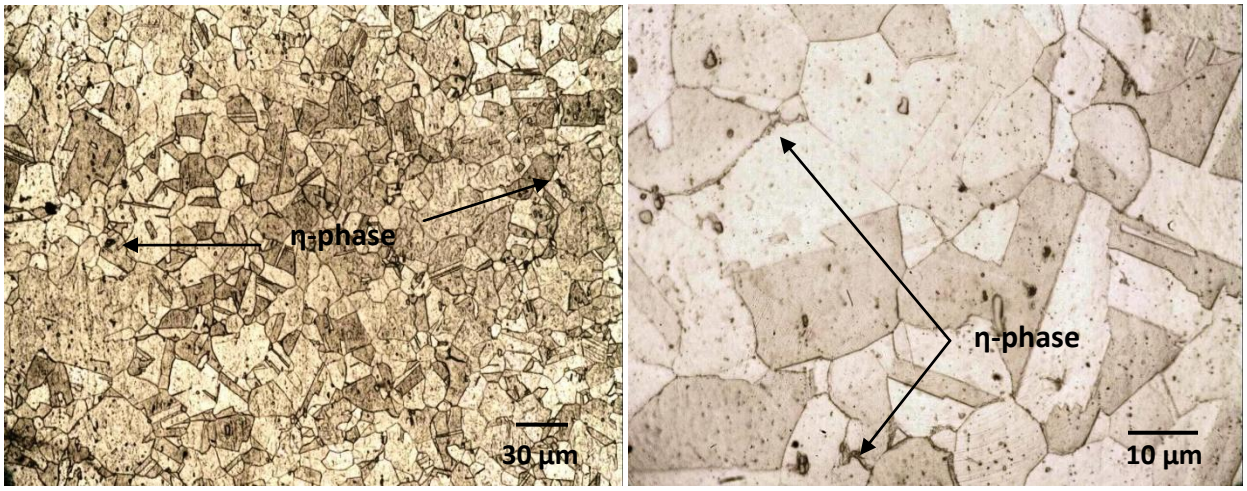

Figure 3.9: Sample 1A5. Arrows indicate the presence of η-phase (Kalling's #2 etch).

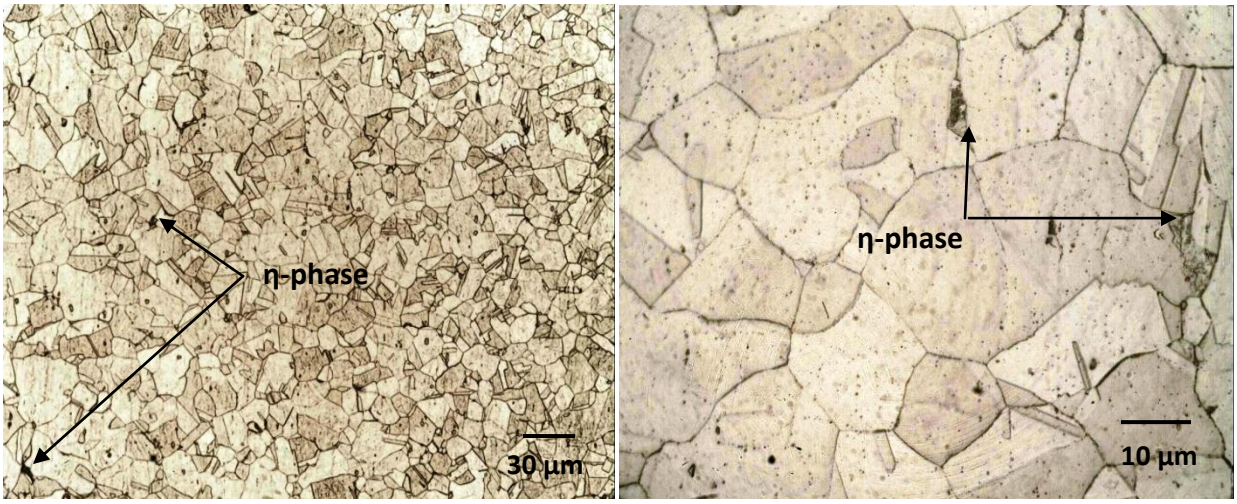

Figure 3.10: Sample 1B5. Arrows indicate the presence of η-phase (Kalling's #2 etch).

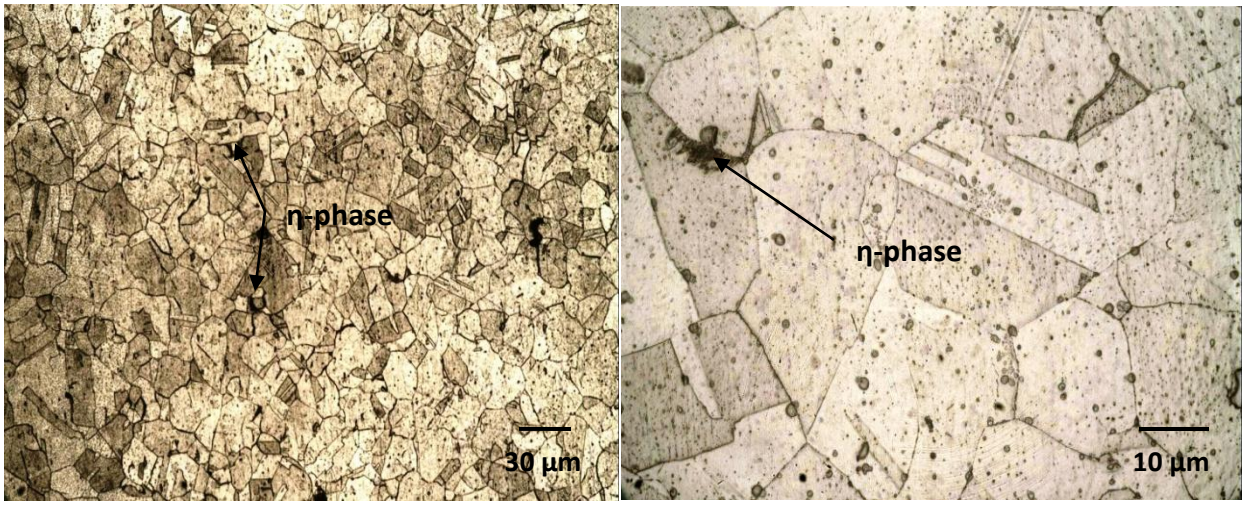

Figure 3.11: Sample 1A6. Arrows indicate the presence of η-phase (Kalling's #2 etch).

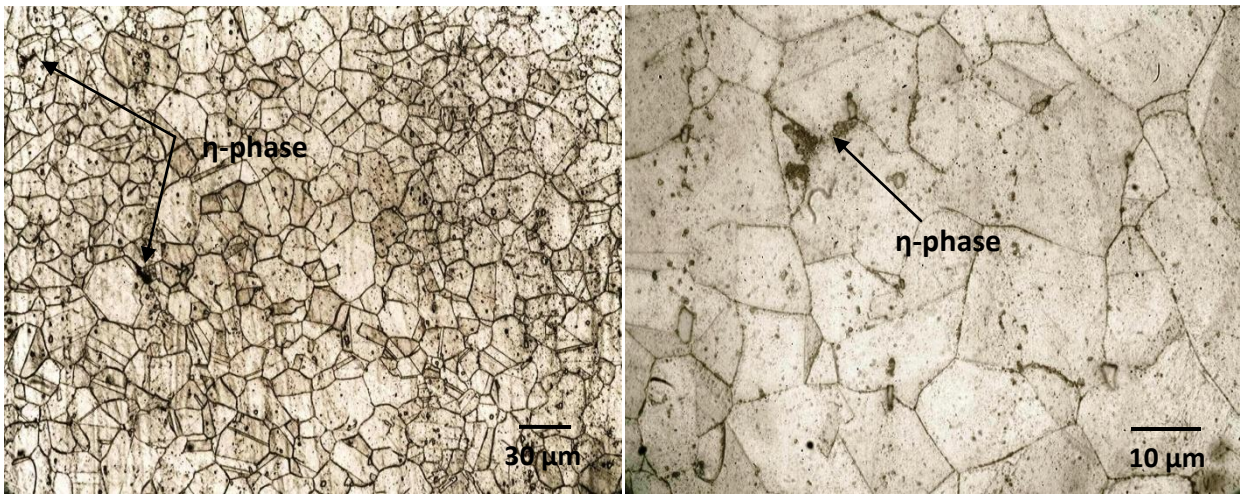

Figure 3.12: Sample 1B6. Arrows indicate the presence of η-phase (Kalling's #2 etch).

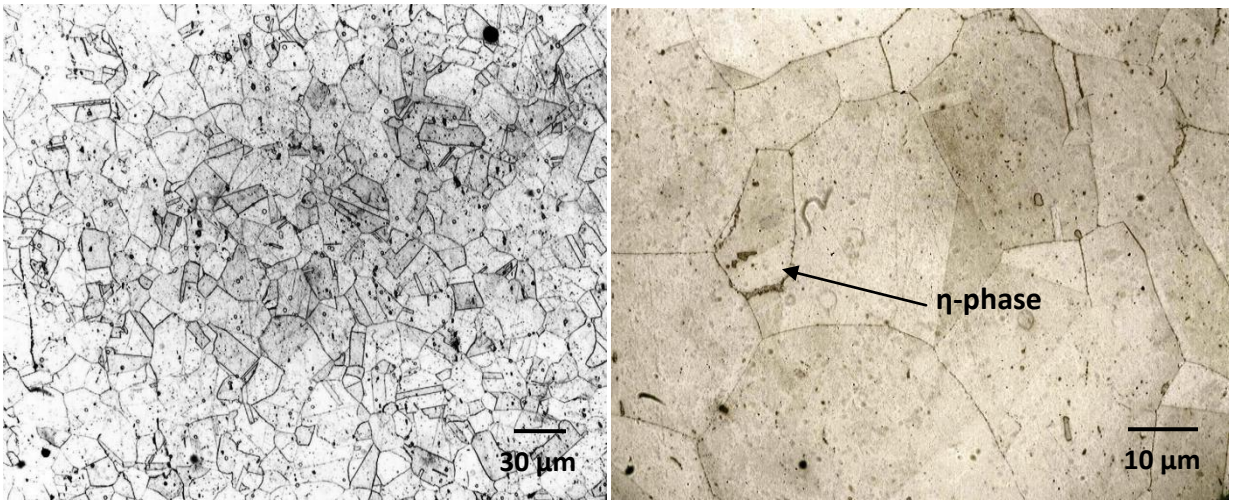

Figure 3.13: Sample 1A7. Arrow indicates the presence of η-phase above the dovetail region (Kalling's #2 etch).

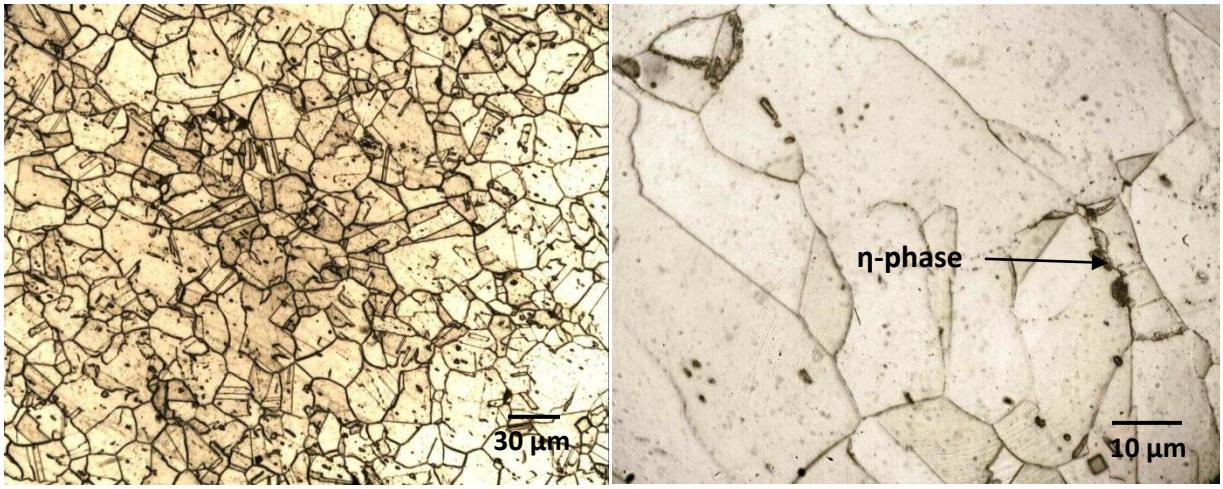

Figure 3.14: Sample 1B7. Arrow indicates the presence of η-phase above the dovetail region (Kalling's #2 etch).

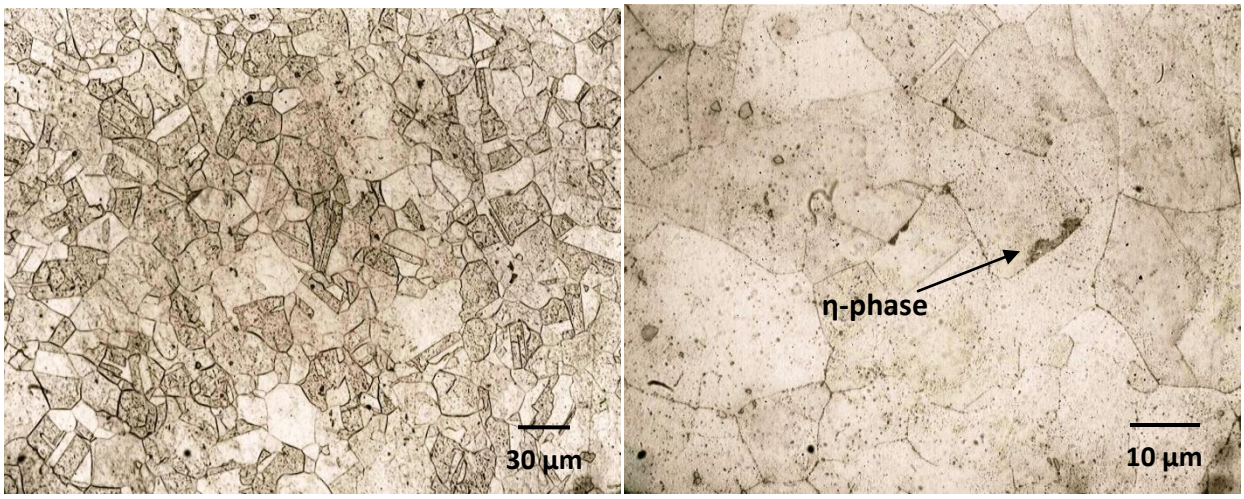

Figure 3.15: Dovetail section 1A8. Arrow indicates the presence of η-phase (Kalling's #2 etch).

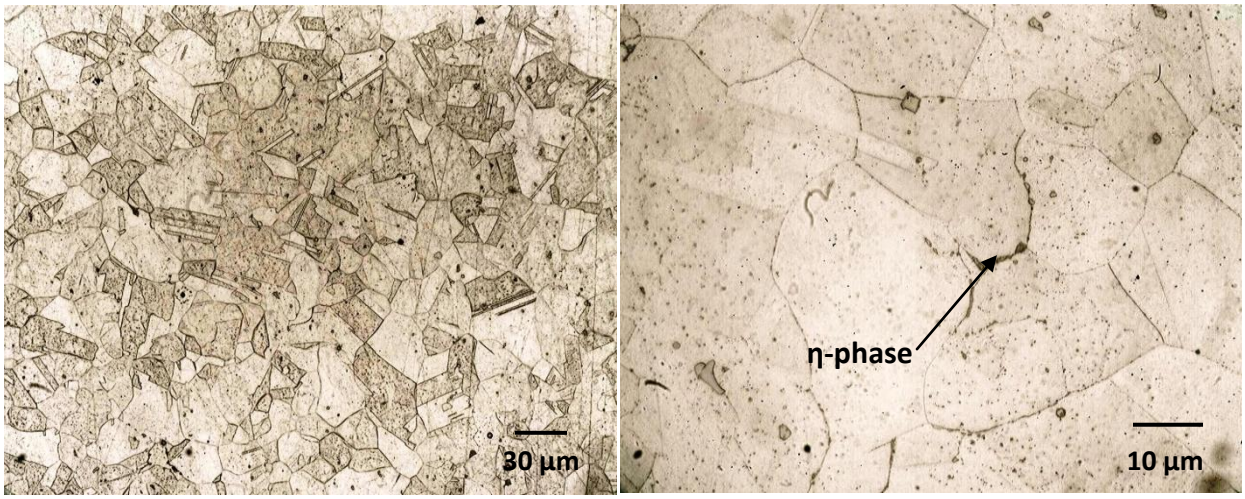

Figure 3.16: Dovetail section 1B8. Arrow indicates the presence of η-phase (Kalling's #2 etch).

Figures 3.17 through 3.20 show the solutionized airfoils. No signs of η-phase were observed anywhere in the microstructure, meaning that η-phase reverted back into solution resulting in a "clean" microstructure.

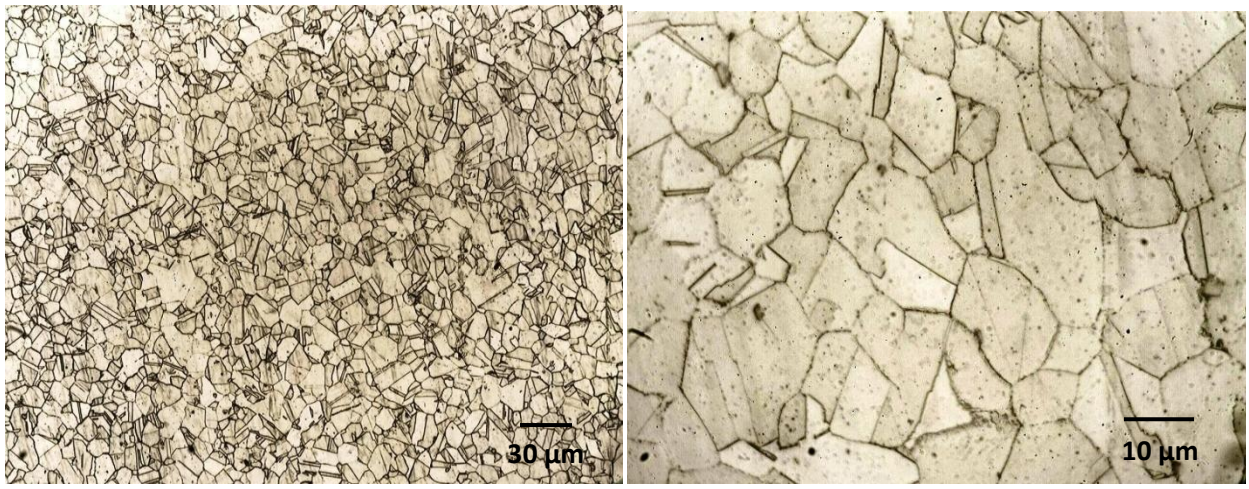

Figure 3.17: Sample 2A1. No presence of η-phase in the solutionized microstructure (Kalling's #2 etch).

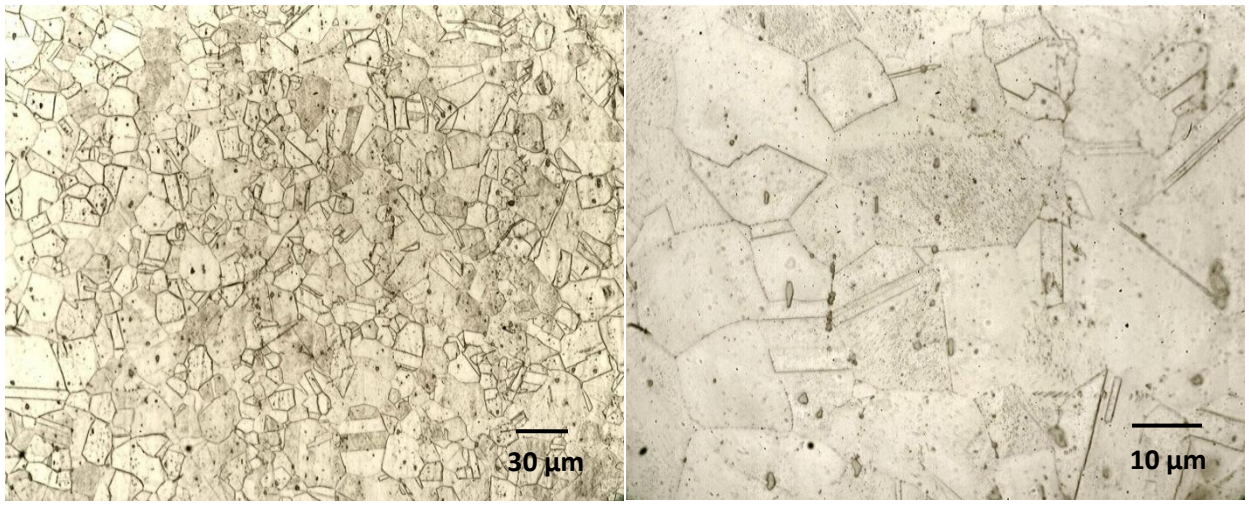

Figure 3.18: Sample 2B1. No presence of η-phase in the solutionized microstructure (Kalling's #2 etch).

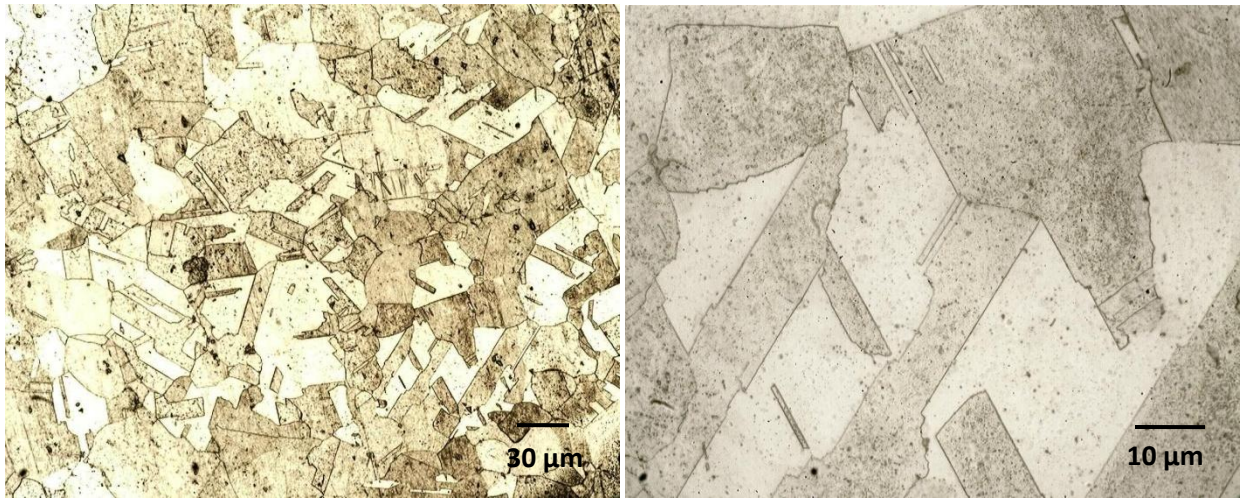

Figure 3.19: Dovetail section 2A8. No presence of η-phase (Kalling's #2 etch).

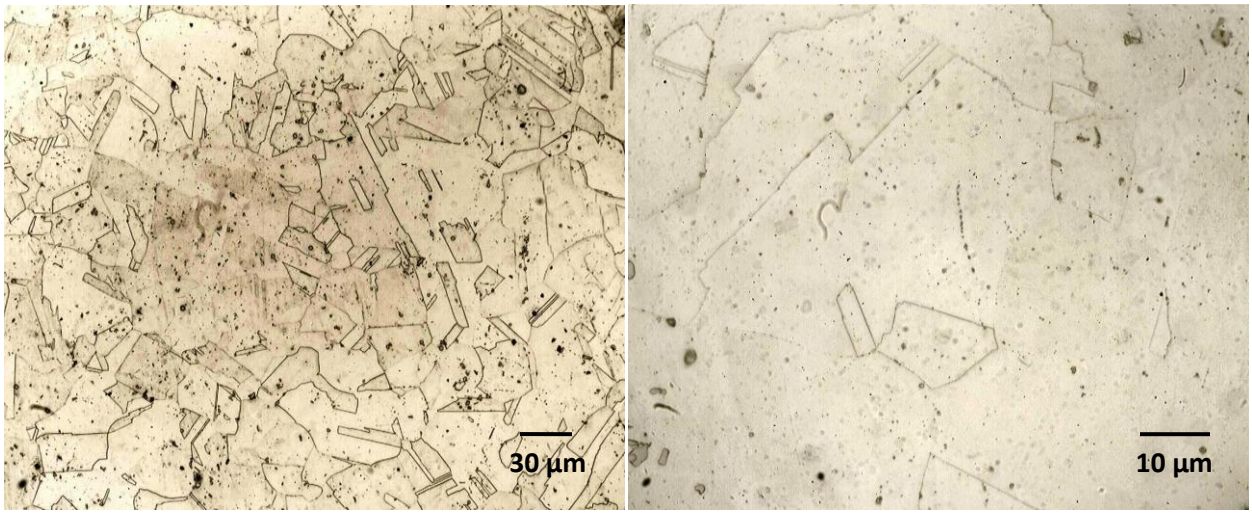

Figure 3.20: Dovetail section 2B8. No presence of η-phase (Kalling's #2 etch).

Figures 3.21 through 3.24 show the specimens after solutionizing and artificially aging. The microstructures are still free from η-phase formation.

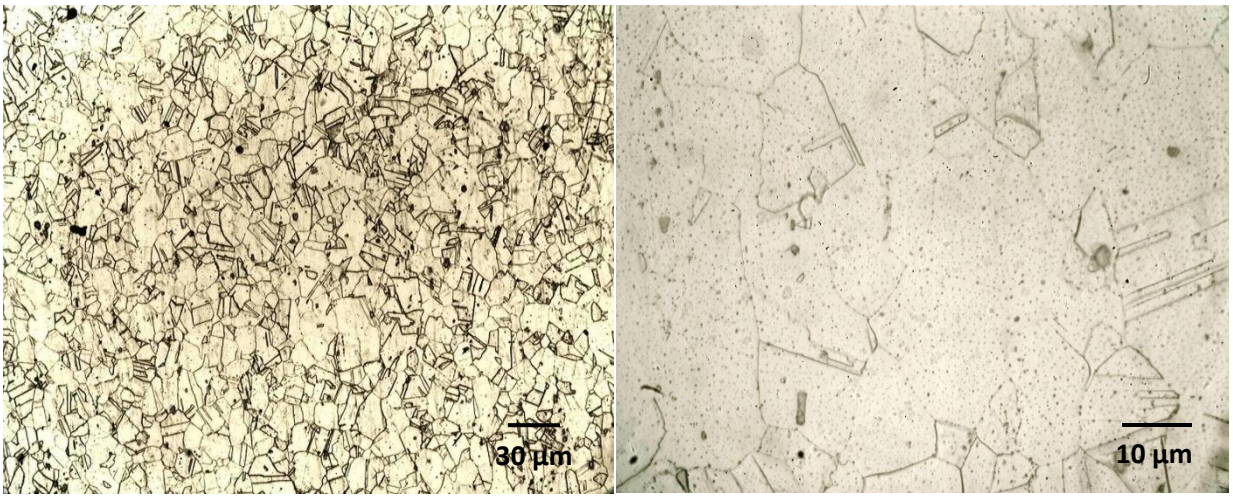

Figure 3.21: Sample 3A1. No presence of η-phase in the airfoil section after aging (Kalling's #2 etch).

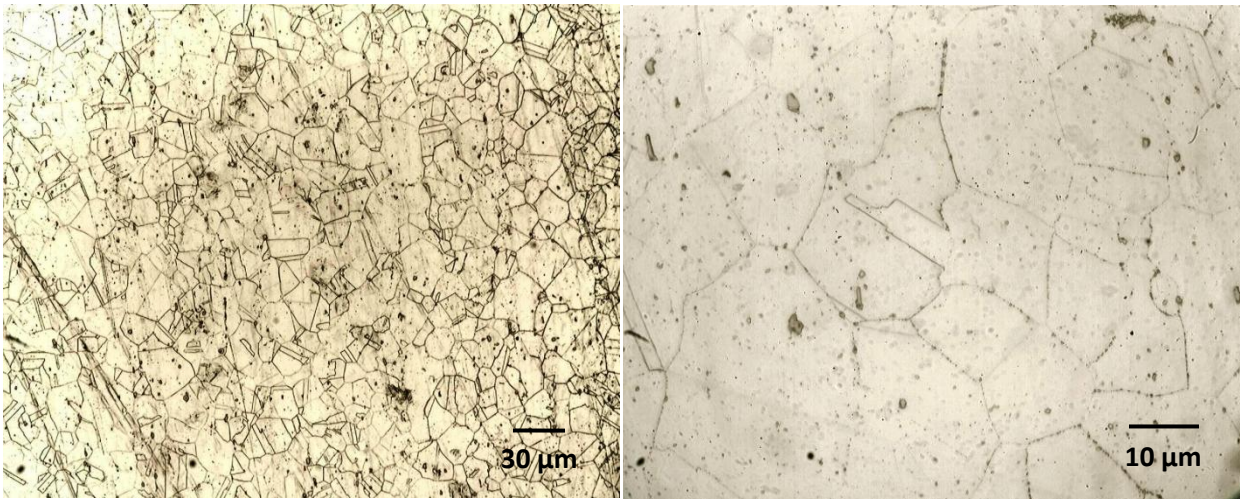

Figure 3.22: Sample 3B1. No presence of η-phase in the airfoil section after aging (Kalling's #2 etch).

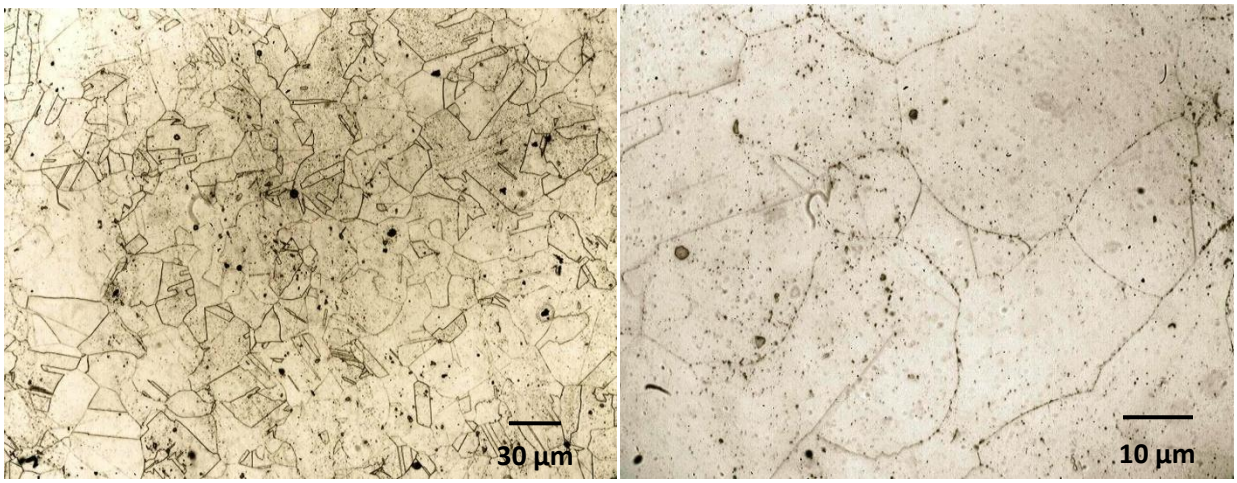

Figure 3.23: Dovetail section 3A8. No presence of η-phase in the dovetail region (Kalling's #2 etch).

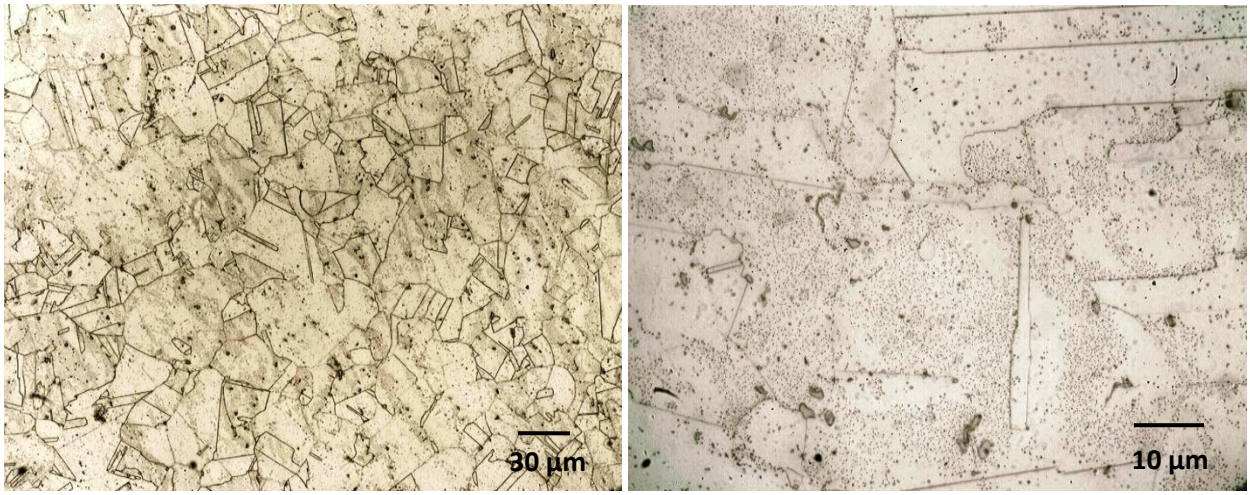

Figure 3.24: Dovetail section 3B8. No presence of η-phase in the dovetail region (Kalling's #2 etch).

SEM was performed on airfoil "A", the airfoil showing a greater abundance of η-phase in the as-received condition, to observe the microstructural effects of the heat

treatment. Figure 3.25 is an overview of the as-received microstructure with evidence of η-phase, $M_{23}C_6$ and MC carbide structures. Electron diffraction spectroscopy (EDS) was used to determine the compositions of some phases.

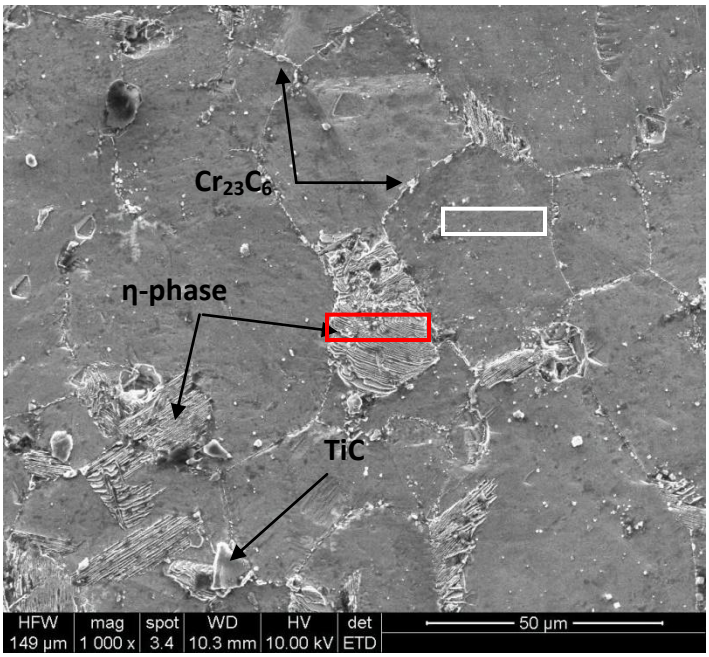

Figure 3.25: As-received microstructure of airfoil "A". Chromium carbides normally form in grain boundaries. The "blocky" structures are primary carbides and the lamellar structure is η-phase. Notice the areas boxed in were used for EDS evaluation.

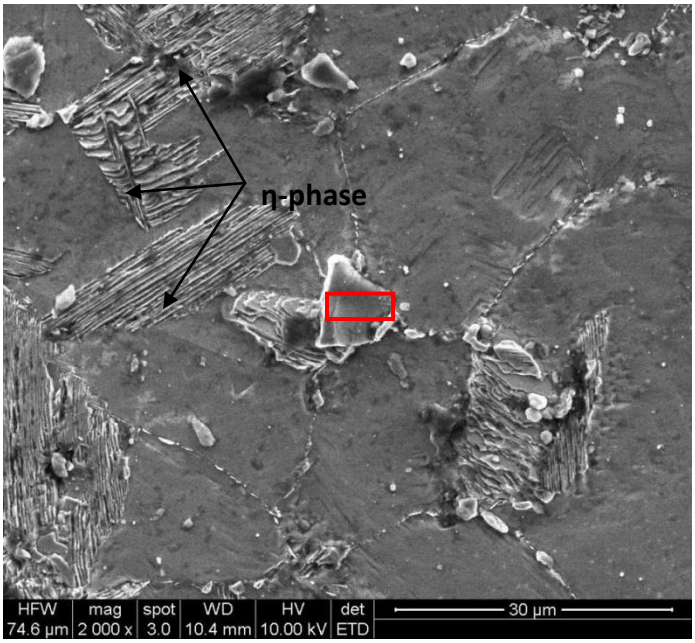

Figure 3.26: SEM photo showing the presence of TiC, η-phase and $Cr_{23}C_6$ in the as-received sample. Notice the area in the red box was used for EDS evaluation.

The SEM photo in Figure 3.26 shows the presence of carbides which were identified as TiC by electron diffraction spectroscopy (EDS) and the results are in Figure 3.27. The results show peaks corresponding to an enrichment of titanium and carbon leading to the conclusion that this is the primary carbide TiC. The carbides that are located within the grain boundaries were too small for EDS to be effective because at such high magnifications the electron beam was hard to stabilize in one area to get accurate peak measurements.

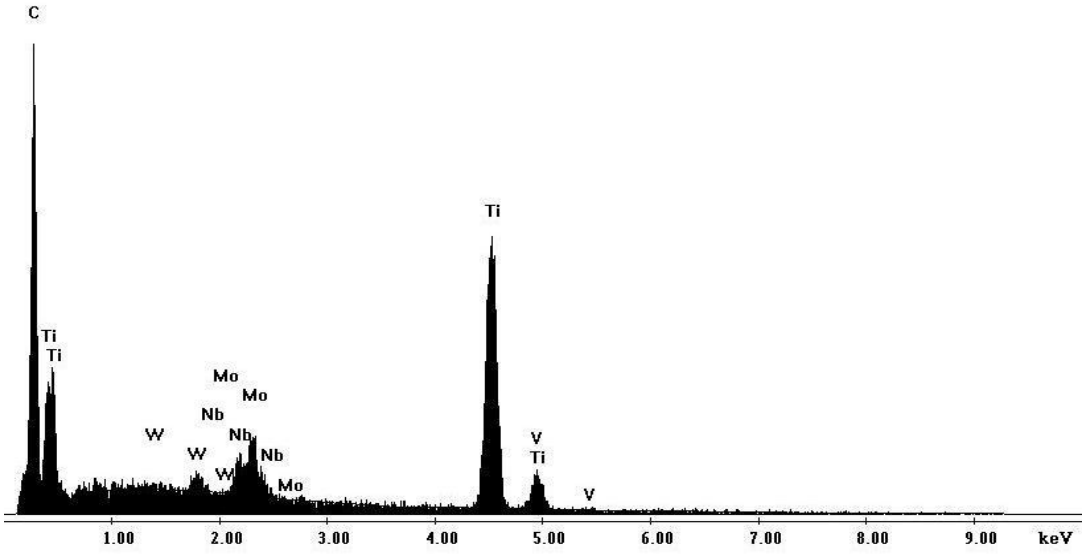

Figure 3.27: EDS preformed on sample in Figure 3.26 showing a Ti-rich carbide phase. The area for evaluation is designated by the red box in Figure 3.26.

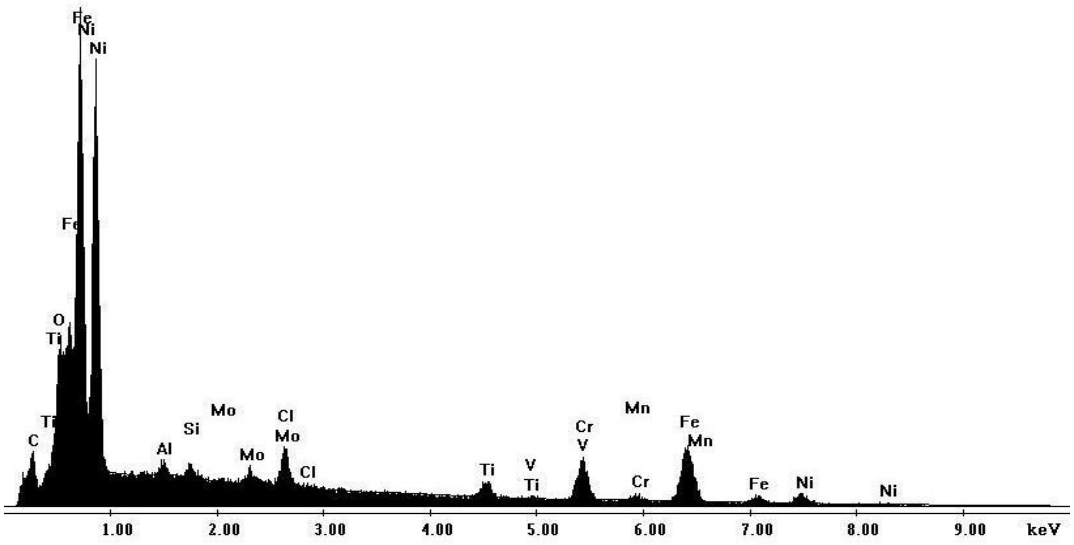

Figure 3.28: EDS preformed on the base material in Figure 3.25 showing high iron and nickel peaks. The area designated by the white box in Figure 3.25 was used for this evaluation.

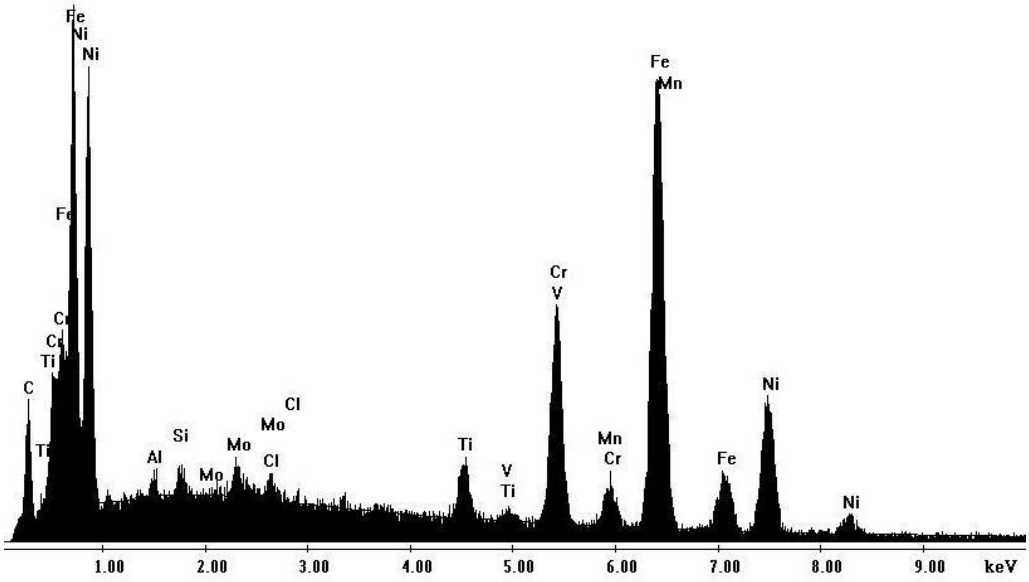

Figure 3.29: EDS preformed on the lamellar structure in Figure 3.25 showing high peaks in iron, chromium, nickel, and titanium. The red box in Figure 3.25 was the area used for this evaluation.

The EDS preformed in Figure 3.29 shows high amounts of titanium, nickel, iron and chromium. Since $M_{23}C_6$ can also form cellular structures like η-phase, then the chances of both phases being detected in this result is also high. With the electron beam moving at the high magnifications that the EDS was being performed at there is a chance that the beam had taken readings from the η-phase and had moved onto the carbide phase.

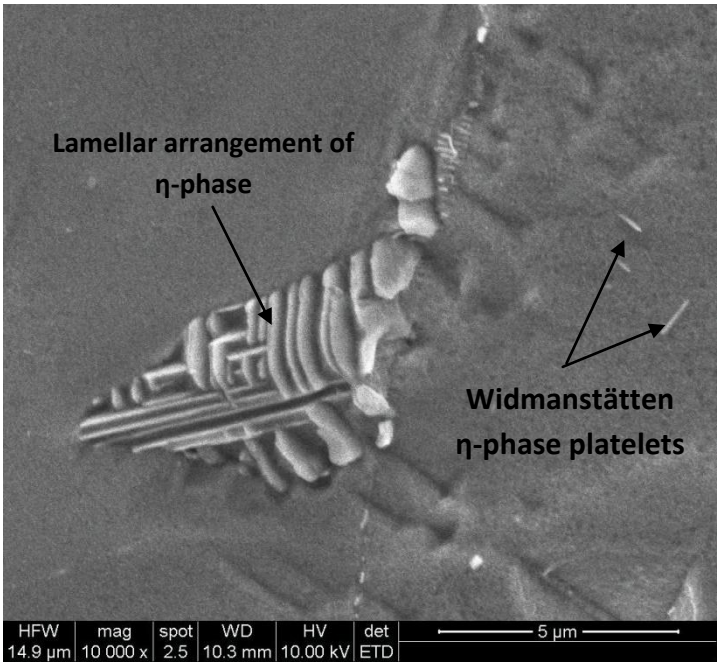

Figure 3.30: High Magnification of η-phase in both Widmanstätten and cellular forms. Notice the lamellar arrangement of η-phase.

The SEM photo in Figure 3.30 shows η-phase in both the Widmanstätten and cellular forms. Figures 3.31 and 3.32 are SEM photos of the microstructure after solution heat treatment. In both photos there were no observations of η-phase. No observations of η-phase were made in Figures 3.33 and 3.34, but observations of γ' were found. The cube-like arrangement that is noticed in Figure 3.34 shows the precipitation of γ' after the solution and aging heat treatment.

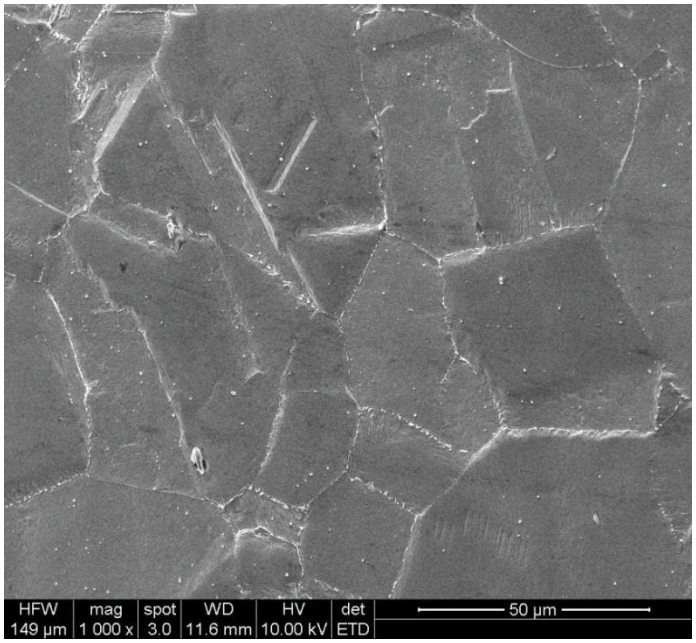

Figure 3.31: SEM photo of the microstructure after solutionizing showing no signs of η-phase.

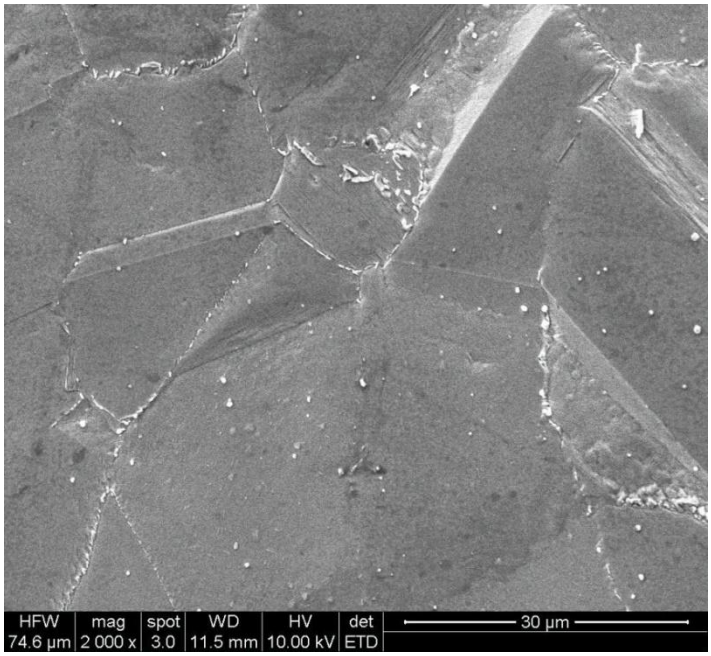

Figure 3.32: SEM photo of the microstructure after solutionizing showing no signs of η-phase.

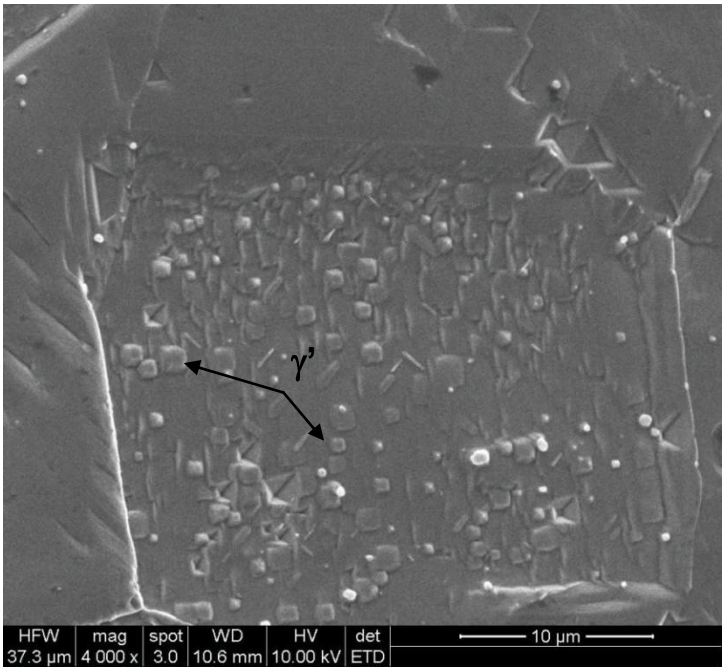

Figure 3.33: SEM photo of the solutionized then aged sample. Arrows indicate the cube-like structures of γ'.

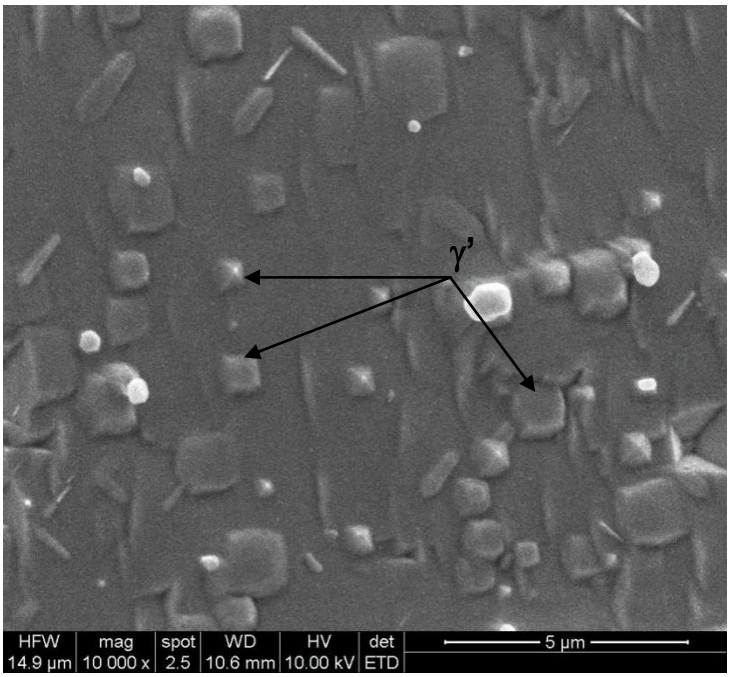

Figure 3.34: Higher magnification of the cubic structures of γ' indicated by the arrows.

To calculate the amount of η-phase present in the airfoils, a one-hundred point grid was used and this method is shown in Figure 3.35. The grid overlapped the optical photographs and each point on the grid that intersected η-phase was counted.

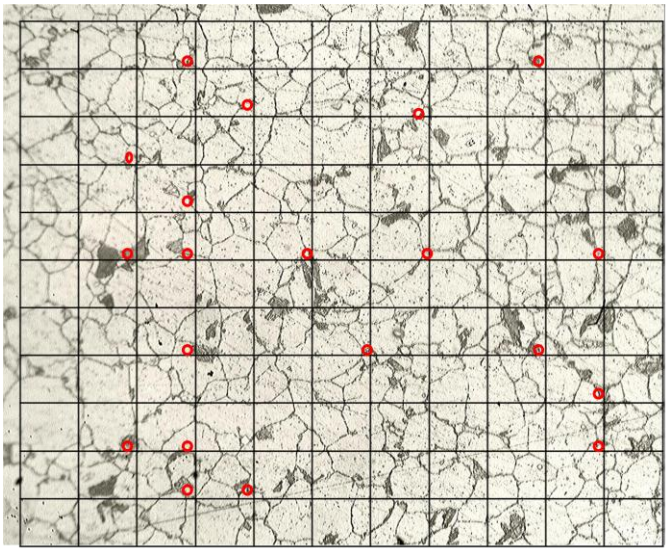

Figure 3.35: The 100-point intersect method performed on the optical microscopy images to determine percentages of η-phase. The circles represent intersections with η-phase.

Table 3.1 shows the percentages of η-phase tabulated in replication and metallographic photos descending from the tip of the turbine airfoil to the dovetail section that connects to the turbine wheel.

Table 3.1: Percent η-phase found in A-286 turbine airfoil investigation for as-received samples

Position	Airfoil A	Airfoil B
	Surface	
Replication (Surface blade tip)	20%	14%
	Volume	
1 (blade tip)	14%	10%
2	6%	6%
3 (wire holes)	8%	7%
4	4%	3%
5	4%	3%
6	3%	2%
7	1%	1%
8 (dovetail region)	1%	1%

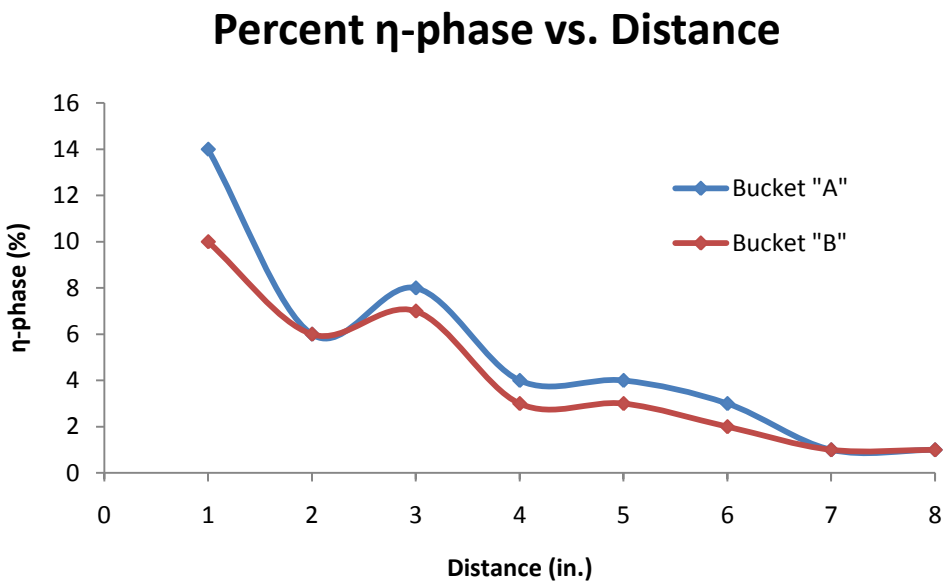

Figure 3.36: Percent η-phase relationship with the thermal gradient of the airfoils. Notice that the amount of η-phase decreases from the blade tip (1) to the dovetail section (8).

Table 3.2 shows the hardness values in both Vickers and Rockwell C (R_C). Hardness was first performed on the airfoil section near the tip followed by hardness measurements on the dovetail region. Vickers hardness values averaged around 354 (35 R_C) for both as-received and aged samples and 197 (10 R_C) for the solutionized samples shows that the material did undergo solutionization and an aging heat treatment. The only two carbides that were big enough to measure hardness were TiC and the Vickers hardness values were 517 (50.6 R_C) and 502 (49.3 R_C). The values show no appreciable change in hardness from the airfoil tip transitioning to the dovetail section. There is also no appreciable difference in the hardness values recorded for the as-received and aged samples. With little difference in these hardness values then it is hard to say if there is an appreciable loss in tensile or stress rupture properties.

Table 3.2: Microhardness values through all three sections of the airfoil

	As-received Vickers (R_C)	Solutionized Vickers (R_C)	Solution/Aged Vickers (R_C)
	Near Blade Tip		
	350 (35.4)	200 (11.1)	333 (33.8)
	347 (35.2)	202 (11.8)	345 (35.0)
	358 (36.4)	196 (10.2)	339 (34.3)
	346 (35.1)	198 (10.7)	354 (35.9)
	353 (35.8)	196 (10.2)	343 (34.8)
AVG. HARDNESS	**350.8**	**198.4**	**342.8**
STD. DEVIATION	**4.868**	**2.608**	**7.759**
	Dovetail Section		
	359 (36.6)	193 (9.4)	354 (35.9)
	330 (33.4)	188 (8.3)	337 (34.1)
	365 (37.3)	201 (11.6)	358 (36.4)
	369 (37.6)	200 (11.1)	334 (33.9)
	343 (34.8)	194 (9.7)	345 (34.9)
AVG. HARDNESS	**353.2**	**195.2**	**345.6**
STD. DEVIATION	**16.3154**	**5.3572**	**10.406**
OVERALL AVG.	**352 (35.76)**	**197 (10.41)**	**345 (34.9)**

Conclusions

This investigation found that the service time of the airfoils is proportional to the amount and size of η-phase found in the airfoil. In the investigation of Airfoils A and B, there was more η-phase found in airfoil “A” than airfoil “B” because airfoil “A” was in service three times longer than airfoil “B”. Both airfoils showed a decrease in percent η-phase when transitioning from the tip of the blade to the dovetail section that attaches to the turbine wheel. This is a phenomenon that is a result of the thermal gradient that the airfoils experience in service. Also, there was a greater amount of η-phase found near the surface regions than was found near the center of the airfoil. This phenomenon is also a result of the temperature gradient that the airfoils experience in service. Also, Airfoil A has a grain size that happens to be noticeably smaller than Airfoil B which could potentially be the reason why more η-phase has formed. Larger grain boundary surface area will result in a greater nucleation and growth of η-phase due to the larger number of nucleation sites.

There seems to be little difference in the hardness results when comparing the hardness of the as-received and the aged stages. Solutionizing the as-received samples dropped the hardness of the alloy due to the γ' going back into solution leaving the alloy with no means of primary strengthening. Once the samples were aged the precipitates formed from solution and the hardness was once again restored. With little appreciable difference in hardness values from the airfoil tip transitioning to the dovetail section shows that the properties are fairly even throughout. With no difference in hardness values comparing as-received and aged sections points at a fact that there could be no appreciable loss in mechanical properties. This could be true if η-phase is

a surface issue because it wouldn't penetrate deep enough to alter those properties even though there would be expectations of alterations at the surface of these components.

Cellular η-phase appears in A-286 as alternate coherent lamellae of η and γ originating at a grain boundary with random orientation with the grain in which it is growing. $M_{23}C_6$ can also form a lamellae structure from the grain boundaries in which it also nucleates and can grow. With cellular formations of $M_{23}C_6$ it is possible to misinterpret it as η-phase.

The rejuvenation process, consisting of a solutionizing and aging treatment, was demonstrated to successfully eliminate η-phase in the microstructure by converting it back into solution and precipitated back out as γ'. With the reverse transformation of η-phase to γ' the "near new" microstructure will also replenish the alloy's mechanical properties. Further work that could be done with more time or material would be to follow up with x-ray diffraction (XRD) and transmission electron microscopy (TEM). The reason for XRD would be to further identify and establish a stronger distinction between the phases. Transmission electron microscopy could be used to further investigate η-phase formation and orientation of growth into γ grains and to further investigate how stacking faults and anti-phase boundaries contribute to η-phase formation.

After making the observation that η-phase seems to be more of a surface deterioration than volumetric. Inspecting these components using in-situ metallurgy isn't giving the operators the insight they need in order to make the decision at whether or not the turbine components are to be removed from service. If replication is

performed to check the integrity of a component and results show a 15-20% η-phase in optical microscopy the operator must realize that those results are for the surface only. The percentile of η-phase actually decreases through the material thickness and it also decreases from the blade tip down to the dovetail section. Further investigation could be performed to test the growth rate of η-phase on the surface compared to the cross-sectional area. This could be used to as a guideline that operators could follow to determine how much η-phase could possibly be present after performing in-situ metallography on the turbine components.

References

1. Sims, Chester T.; Hagel, William C. The Superalloys. Pg. 17. John Wiley & Sons. 1972.
2. Personal contact
3. R. F. Decker and R. R. DeWitt, Trends in High-Temperature Alloys, *J. Met.*, **17**, 139-145, February 1965.
4. Y. Han, P. Deb, and M. C. Chaturvedi, Coarsening behavior of γ'- and γ"-particles in Inconel alloy 718, *Met. Sci.*, **16**, 555, (1982).
5. C. P. Sullivan and M. J. Donachie, Jr., Some Effects of Microstructure on the Mechanical Properties of Nickel-Base Superalloys, *Met. Eng. Q.,* **11**, 1-11, (1971).
6. United Performance Metals Technical Data Sheet, Ferguson Metals Inc, Hamilton, OH
7. F. G. Wilson, and F. B. Pickering, Some Aspects of the Deformation of an Age-Hardened Austenitic Steel, *JISI*, **207**, 490-499, (1969).
8. G. N. Maniar and H. M. James, Notch Sensitivity in A-286 Alloy, *Trans. ASM*, **57**, 368-370, (1964).
9. G. B. Heydt, Investigation of Notch Sensitivity in A-286 Alloy, *Trans. ASM*, **54**, 220-226, (1961).
10. B. R. Clark and F. B. Pickering, Precipitation Effects in Austenitic Stainless Steels Containing Titanium and Aluminum Additions, *JISI*, **205**, 70-84, (1967).
11. G. R. Speich: ibid, 1963, **227**, 754.
12. C. S. Smith: Acta. Met., 1955, **3**.

13. K. J. Irvine, D. T. Llewellyn, and F. B. Pickering, High-strength austenitic stainless steels, *JISI*, **199**, 153-175, (1961).
14. Sims, Chester T.; Stoloff, Norman S.; Hagel, William C. Superalloys II. Pg. 24, 61, 88 and 165-187. John Wiley & Sons. 1987.

Curriculum Vita

Christopher Michael Bradley was born in El Paso, Texas in the summer of 1980. The first son of Michael Joseph Bradley and Barbara Selma Bradley, he graduated from Irvin High School, El Paso, Texas, in the spring of 1998 and entered The University of Texas at El Paso in the fall of 1998. While pursuing a bachelor's degree in Computer Science, he worked full time at the El Paso International Airport as well as doing landscaping for the American Heart Association on the weekends. He soon changed his major to Metallurgical and Materials Engineering where he received his Bachelor of Science degree from The University of Texas at El Paso in the spring of 2006. He entered graduate school at The University of Texas at El Paso in the fall of 2006 while working as a teaching assistant for The University of Texas at El Paso in the engineering program. He also began work with Herrera, Stafford & Associates (HS&A), a consulting firm in El Paso, Texas, starting in 2006 through 2009 performing failure investigations and characterization. He received his Master of Science degree in 2009 and is a current member of Alpha Sigma Mu and The National Scholars Honor Society.

Permanent Address: 9000 Virgo Ln.

El Paso, Texas 79904